AD-A124 576 THE EFFECT OF UNIFORM FLOW ON THE DYNAMICS AND ACOUSTICS OF FORCE-EXCITED..(U) ADMIRALTY MARINE TECHNOLOGY ESTABLISHMENT TEDDINGTON (ENGLAND.. 1/1

UNCLASSIFIED D J ATKINS DEC 82 AMTE(N)/TM82087 F/G 13/10 NL

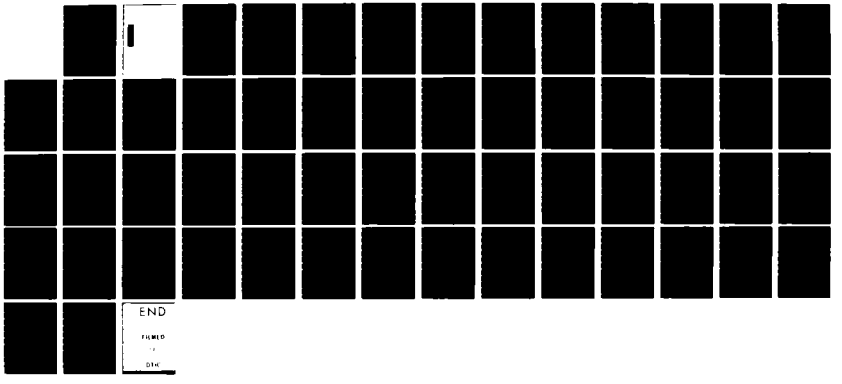

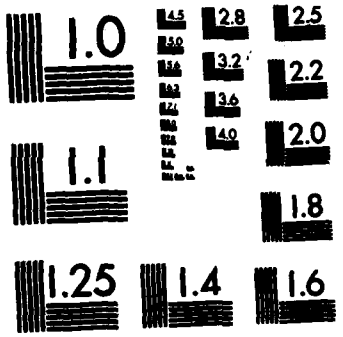

AMTE(N)TM82087

THE EFFECT OF UNIFORM FLOW ON THE DYNAMICS AND ACOUSTICS OF FORCE-EXCITED INFINITE PLATES

BY

D J ATKINS

Summary

Formulae are obtained for the time-harmonic steady-state plate displacement, acoustic pressure and particle velocities. The far-field pressure is obtained from a stationary phase approximation, and two separate formulations are used to define a time-averaged acoustic intensity vector. The stability of a line-excited plate is examined using both a steady-state approach and a causal approach which is able to distinguish between absolute and convective instability. Some numerical results are presented for a steel plate vibrating in water. The far-field pressure is not significantly affected by flow speeds of a practical magnitude. The very low-frequency acoustic intensity vectors at the plate surface are affected considerably, but at higher frequencies there is no significant effect. At low flow speeds a convective instability is found and at higher flow speeds there is an absolute instability.

AMTE (Teddington)
Queen's Road
TEDDINGTON Middx TW11 0LN

62 pages
19 figures

December 1982

CONTENTS

LIST OF SYMBOLS

c	speed of sound in fluid
c_p	phase speed of free waves in plate-fluid system
c_0	phase speed of free waves along plate in vacuo
D	bending stiffness of plate $[=Eh^3/\{12(1-\nu^2)\}]$
E	plate Young's modulus
f	frequency in Hz
F_0	point force or line force per unit length
h	plate thickness
i	$\sqrt{(-1)}$
$\vec{I}$	acoustic intensity vector
I_x, I_y, I_z	components of acoustic intensity vector
Im[ ]	imaginary part
k	wavenumber in fluid $(=\omega/c)$
k_p	free plate wave number $\{=(\rho_s h\omega_0^2/D)^{1/4}\}$
M	Mach number $(=U/c)$
$\vec{N}$	energy flux vector
N_x, N_y, N_z	components of energy flux vector
p	instantaneous value of acoustic pressure
P	acoustic pressure amplitude
R	radial distance from excitation
Re[ ]	real part
t	time
U	flow speed
v_x, v_y, v_z	instantaneous values of acoustic particle velocity
V_x, V_y, V_z	acoustic particle velocity amplitudes
$w(x,y,t)$	instantaneous value of plate displacement
$W(x,y)$	plate displacement amplitude (point-force excitation)
$W(x)$	plate displacement amplitude (line-force excitation)
$W(x,t)$	plate displacement amplitude (line-force excitation, causal approach)
$\bar{W}$	Fourier transform of W or $\tilde{W}$
$\tilde{W}$	Laplace transform of W

x,y,z	rectangular Cartesian co-ordinates
$Z(\omega,\alpha,\beta)$	dispersion function for a point-excited plate
$Z(\omega,\alpha)$	dispersion function for a line-excited plate
α,β	Fourier transform wave numbers (α only for line-excited plates)
$\gamma(\alpha,\beta)$	Fourier transform wavenumber of acoustic pressure and acoustic velocity potential
$\delta(\ )$	delta function
ζ	dimensionless wavenumber
η	plate loss factor
θ	angle in cylindrical and spherical co-ordinate system
μ	fluid-loading parameter ($=\rho/\rho_S h$)
ν	Poisson's ratio for plate
ρ	fluid density
ρ_S	plate material density
σ	$\mathrm{Im}[\omega]=\sigma$ denotes line of Laplace integration
φ	instantaneous value of acoustic velocity potential
Φ	amplitude of acoustic velocity potential
Ψ	angle in spherical co-ordinate system
ω,ω_0	radian frequency ($=2\pi f$)
*	(as superscript) denotes complex conjugate

INTRODUCTION

Much theoretical work has been carried out on the dynamics of point- and line-excited infinite fluid-loaded plates, with the fluid assumed to be stationary [1-7]. In practice however, either the plate or the fluid may be in motion and hence an understanding of the effect of flow on the properties of such dynamical systems is required. Here, expressions are derived for the plate response and radiated sound pressure for point- and line-excited infinite plates in the presence of a uniform inviscid flow. The expressions are obtained as one- and two-dimensional Fourier integrals over a wavenumber space, by solving the steady-state equations of motion using Fourier transforms.

There has been much debate in the literature over the past twenty years on a theoretical definition of acoustic intensity in the presence of flow, with particular application to duct acoustics. There has also been a recent interest in the measurement of acoustic intensity rather than just the sound pressure level as such measurements indicate the direction of acoustic energy flow. At AMTE, Spicer [8] has numerically computed and plotted acoustic intensity vectors in the near field of a line-excited plate without flow. It is difficult to attach a meaning to the term "acoustic intensity" in situations where there is mean flow. However, two definitions of the acoustic intensity vector have been proposed and discussed in the literature [9-12], both of which satisfy a conservation relation, i.e. the net outflow of acoustic energy from any volume equals the rate of decrease of the acoustic energy contained within that volume. In the present study, the work of Spicer has been extended to include the effect of uniform flow. Intensity vectors are evaluated numerically using both definitions and the results are compared.

In the absence of flow, the only source of energy in the plate/fluid system is the exciting force. Hence the net acoustic energy flow is outwards from this force. Without plate damping, free waves must either propagate or decay away from the excitation. A moving fluid possesses energy and hence energy transfer between the plate and the fluid or vice versa may give rise to instabilities. The general problem of the effect of a flexible boundary on hydrodynamic stability has been studied by Benjamin [13,14], Landahl [15], Miles [16] and others. These workers found theoretically that there are three different types of instability possible, denoted by them as classes A, B and C. Class A disturbances are the Tollmein-Schlichting waves encountered in stability treatments of flow over a rigid surface; these disturbances are modified by the presence of a flexible boundary and destabilized by damping. Class B disturbances are free surface waves which can propagate along the boundary if the fluid is absent but which are modified by the reaction of the disturbed flow. Class C disturbances are analogous to the Kelvin-Helmholtz instability associated with vortex sheets and these

disturbances occur when conservative hydrodynamic forces cause a unidirectional transfer of energy to the boundary. Gupta et al. [17] in a laboratory experiment observed class A and class B instabilities on an air-water interface. Class A waves could be excited at low air speeds by a ribbon vibrating in the air and the class B waves at slightly higher speeds by a ribbon vibrating in the water. There was some evidence of class C instability at still higher air speeds.

An alternative approach to stability was adopted by Melcher [18] in consideration of wave propagation in flows with electric and magnetic fields. He applied the principle of causality, i.e. that the system remains undisturbed until at some instant an excitation is suddenly applied, and the system response is then calculated after a long time interval. There are three possibilities: first that the response at all points of the system consists of components represented by propagating or decaying waves, secondly that the response at all points may increase exponentially with time, and thirdly that the response contains a propagating wave which increases in amplitude with distance although the response at a fixed point does not amplify with time. These three possibilities are usually termed "stable", "absolutely unstable" and "convectively unstable" respectively.

Brazier-Smith & Scott [19], using a causal approach, have examined theoretically the stability of uniform incompressible flow over a line-excited undamped infinite plate. They deduced a critical flow speed above which the system is absolutely unstable and below which the downstream response exhibits a convective instability. In the present work, similar results have been obtained numerically for compressible flow, and the effect of plate damping on stability is considered. The causal approach and the Benjamin-Landahl approach to stability are compared and shown to give similar results at low flow speeds, but different results at high flow speeds.

2. POINT-EXCITED INFINITE PLATE

A uniform thin plate lies in the plane $z=0$ and it is subjected to a time-harmonic point force given by

$$\mathrm{Re}[F_0 \exp(-i\omega_0 t)]$$

at the origin. The half-space $z>0$ is occupied by an inviscid compressible fluid moving with constant velocity $U=Mc$ in the x-direction, where M is a dimensionless Mach number. The region $z<0$ is in a vacuum. The Cartesian co-ordinates x, y and z are assumed to be stationary (i.e. not moving with the fluid). Figure 1(a) shows the geometry of interest.

Let $w(x,y,t)$, $p(x,y,z,t)$ and $\varphi(x,y,z,t)$ be the instantaneous values of plate displacement, acoustic pressure and acoustic velocity potential, respectively. Then the plate equation of motion is

$$\begin{aligned} &D[\{(\partial^2/\partial x^2) + (\partial^2/\partial y^2)\}^2 + \rho_s h(\partial^2/\partial t^2)]w \\ &= \mathrm{Re}[F_0 \exp(-i\omega_0 t)]\cdot\delta(x)\cdot\delta(y) - p(x,y,0,t) \end{aligned} \tag{1}$$

and the linearized convected form of the acoustic wave-equation is

$$\nabla^2\varphi = (1/c^2)[(\partial/\partial t)+U(\partial/\partial x)]^2\varphi \tag{2}$$

The boundary condition at the plate surface, reflecting continuity of displacement, is

$$(\partial\varphi/\partial z)(x,y,0,t) = -\rho[(\partial/\partial t) + U(\partial/\partial x)]w \tag{3}$$

and the acoustic pressure p can be expressed in terms of the potential φ as

$$p = -\rho[(\partial/\partial t) + U(\partial/\partial x)]\varphi \tag{4}$$

By defining complex amplitudes $W(x,y)$, $P(x,y,z)$ and $\Phi(x,y,z)$ of w, p and φ such that

$$w(x,y,t) = \mathrm{Re}[W(x,y)\cdot\exp(-i\omega_0 t)]$$

(with similar expressions for p and φ), and expressing W, P and Φ as Fourier transforms,

$$W(x,y) = (1/4\pi^2) \iint_{-\infty}^{\infty} \bar{W}(\alpha,\beta)\exp(i\alpha x+i\beta y)\, d\alpha d\beta \tag{5}$$

$$\begin{vmatrix} P(x,y,z) \\ \Phi(x,y,z) \end{vmatrix} = (1/4\pi^2) \iint_{-\infty}^{\infty} \begin{vmatrix} \bar{P}(\alpha,\beta,z) \\ \bar{\Phi}(\alpha,\beta,z) \end{vmatrix} \exp(i\alpha x+i\beta y)\, d\alpha d\beta \tag{6}$$

the solution for these variables can be shown to be

$$W(x,y) = (F_0/4\pi^2) \iint_{-\infty}^{\infty} \frac{\exp(i\alpha x+i\beta y)}{Z(\omega_0,\alpha,\beta)}\, d\alpha d\beta \tag{7}$$

$$P(x,y,z) = (-i\rho\omega_0^2 F_0/4\pi^2) \iint_{-\infty}^{\infty} \frac{(1-\alpha M/k)^2}{\gamma} \frac{\exp(i\alpha x+i\beta y+i\gamma z)}{Z(\omega_0,\alpha,\beta)}\, d\alpha d\beta \tag{8}$$

$$\Phi(x,y,z) = (-\omega_0 F_0/4\pi^2) \iint_{-\infty}^{\infty} \frac{(1-\alpha M/k)}{\gamma} \frac{\exp(i\alpha x+i\beta y+i\gamma z)}{Z(\omega_0,\alpha,\beta)}\, d\alpha d\beta \tag{9}$$

where

$$Z(\omega_0,\alpha,\beta) = D(\alpha^2+\beta^2)^2 - \rho_S h\omega_0^2 - i\rho\omega_0^2(1-\alpha M/k)^2/\gamma \tag{10}$$

is the dispersion relation and

$$\gamma = \sqrt{\{k^2(1-\alpha M/k)^2 - \alpha^2 - \beta^2\}}, \qquad \alpha^2+\beta^2 < k^2(1-\alpha M/k)^2 \tag{11}$$

$$\gamma = i\sqrt{\{\alpha^2+\beta^2 - k^2(1-\alpha M/k)^2\}}, \qquad \alpha^2+\beta^2 > k^2(1-\alpha M/k)^2 \tag{12}$$

to satisfy the radiation condition for outgoing waves.

The acoustic velocity amplitudes, V_x, V_y and V_z (or $\partial\Phi/\partial x$, $\partial\Phi/\partial y$ and $\partial\Phi/\partial z$) are given by

$$V_x = (-i\omega_0 F_0/4\pi^2) \iint_{-\infty}^{\infty} \frac{\alpha(1-\alpha M/k)}{\gamma} \frac{\exp(i\alpha x+i\beta y+i\gamma z)}{Z(\omega_0,\alpha,\beta)} \, d\alpha d\beta \qquad (13)$$

$$V_y = (-i\omega_0 F_0/4\pi^2) \iint_{-\infty}^{\infty} \frac{\beta(1-\alpha M/k)}{\gamma} \frac{\exp(i\alpha x+i\beta y+i\gamma z)}{Z(\omega_0,\alpha,\beta)} \, d\alpha d\beta \qquad (14)$$

$$V_z = (-i\omega_0 F_0/4\pi^2) \iint_{-\infty}^{\infty} (1-\alpha M/k) \frac{\exp(i\alpha x+i\beta y+i\gamma z)}{Z(\omega_0,\alpha,\beta)} \, d\alpha d\beta \qquad (15)$$

3. LINE-EXCITED INFINITE PLATE

The geometry of interest is shown as Figure 1(b). The plate displacement W, the acoustic pressure P, the acoustic potential Φ and the particle velocities V_x and V_z are derived via the one-dimensional Fourier transform as

$$W(x) = (F_0/2\pi) \int_{-\infty}^{\infty} \frac{\exp(i\alpha x)}{Z(\omega_0,\alpha)} \, d\alpha \qquad (16)$$

$$P(x,z) = (-i\rho\omega_0^2 F_0/2\pi) \int_{-\infty}^{\infty} \frac{(1-\alpha M/k)^2}{\gamma} \frac{\exp(i\alpha x+i\gamma z)}{Z(\omega_0,\alpha)} \, d\alpha \qquad (17)$$

$$\Phi(x,z) = (-\omega_0 F_0/2\pi) \int_{-\infty}^{\infty} \frac{(1-\alpha M/k)}{\gamma} \frac{\exp(i\alpha x+i\gamma z)}{Z(\omega_0,\alpha)} \, d\alpha \qquad (18)$$

$$V_x = (-i\omega_0 F_0/2\pi) \int_{-\infty}^{\infty} \frac{\alpha(1-\alpha M/k)}{\gamma} \frac{\exp(i\alpha x+i\gamma z)}{Z(\omega_0,\alpha)} \, d\alpha \qquad (19)$$

$$V_z = (-i\omega_0 F_0/2\pi) \int_{-\infty}^{\infty} (1-\alpha M/k) \frac{\exp(i\alpha x+i\gamma z)}{Z(\omega_0,\alpha)}\, d\alpha \qquad (20)$$

where

$$Z(\omega_0,\alpha) = D\alpha^4 - \rho_S h\omega_0^2 - i\rho\omega_0^2(1-\alpha M/k)^2/\gamma \qquad (21)$$

and

$$\gamma = \sqrt{\{k^2(1-\alpha M/k)^2-\alpha^2\}}, \qquad |\alpha| < k|1-\alpha M/k| \qquad (22)$$

$$\gamma = i\sqrt{\{\alpha^2-k^2(1-\alpha M/k)^2\}}, \qquad |\alpha| > k|1-\alpha M/k| \qquad (23)$$

4. DEFINITION OF THE ACOUSTIC INTENSITY VECTOR

The acoustic intensity vector $\vec{I}$ is defined as the time-average of the instantaneous acoustic intensity or acoustic energy flux vector $\vec{N}$.

$$\vec{I} = \lim_{T\to\infty} \{(1/T)\int_{-\infty}^{\infty} \vec{N}\, dt\} \qquad (24)$$

The problem of defining the vector $\vec{N}$ in a moving acoustic medium has been a subject for debate in the literature [9-12]. Two alternative definitions of $\vec{N}$ have been proposed, both of which satisfy a conservation equation, viz.

$$\partial E/\partial t + \text{div}\, \vec{N} = 0 \qquad (25)$$

where E is the instantaneous acoustic energy density. The first definition (referred to by using subscript 1), according to Morfey [10], gives the following expressions for E_1 and the components N_{x1}, N_{y1} and N_{z1} of N_1

$$E_1 = \tfrac{1}{2}\rho\{(\nabla\varphi)^2 + (1/c^2)(\varphi_t+U\varphi_x)^2 - (2U/c^2)\varphi_x(\varphi_t+U\varphi_x)\} \qquad (26a)$$

$$N_{x1} = -\rho\varphi_t\{(1-U^2/c^2)\varphi_x - (U/c^2)\varphi_t\} \qquad (26b)$$

$$N_{y1} = -\rho\varphi_t\varphi_y \qquad (26c)$$

$$N_{z1} = -\rho\varphi_t\varphi_z \qquad (26d)$$

The second definition (using subscript 2), according to Ryshov & Shefter [9], is

$$E_2 = \tfrac{1}{2}\rho\{(\nabla\varphi)^2 + (1/c^2)(\varphi_t + U\varphi_x)^2\} \tag{27a}$$

$$N_{x2} = -\rho(\varphi_t + U\varphi_x)\varphi_x + \tfrac{1}{2}\rho U\{(\nabla\varphi)^2 + (1/c^2)(\varphi_t + U\varphi_x)^2\} \tag{27b}$$

$$N_{y2} = -\rho(\varphi_t + U\varphi_x)\varphi_y \tag{27c}$$

$$N_{z2} = -\rho(\varphi_t + U\varphi_x)\varphi_z \tag{27d}$$

In the above expressions, subscripts t, x, y and z of φ denote partial derivatives with respect to time and the co-ordinate directions respectively.

The quantities E_i and N_i (i=1,2) can be expressed in terms of the instantaneous acoustic pressure p and velocity components v_x, v_y and v_z as

$$E_1 = p^2/(2\rho c^2) + (U/c^2)pv_x + \tfrac{1}{2}\rho(v_x^2+v_y^2+v_z^2) \tag{28a}$$

$$N_{x1} = pv_x(1+M^2) + (M/\rho c)p^2 + \rho U v_x^2 \tag{28b}$$

$$N_{y1} = (p+\rho U v_x)v_y \tag{28c}$$

$$N_{z1} = (p+\rho U v_x)v_z \tag{28d}$$

$$E_2 = p^2/(2\rho c^2) + \tfrac{1}{2}\rho(v_x^2+v_y^2+v_z^2) \tag{29a}$$

$$N_{x2} = pv_x + (M/2\rho c)p^2 + \tfrac{1}{2}\rho U(v_x^2+v_y^2+v_z^2) \tag{29b}$$

$$N_{y2} = pv_y \tag{29c}$$

$$N_{z2} = pv_z \tag{29d}$$

It should be noted that the expressions for the components of $\vec{N}_1$ and $\vec{N}_2$ reduce to well-known expressions in the absence of flow (U=M=0).

The components of the time-averaged intensity vector $\vec{I}$ according to formulations 1 and 2 are, in terms of the complex amplitudes P, V_x, V_y and V_z,

$$I_{x1} = \tfrac{1}{2}\mathrm{Re}[\{P(1+M^2)+\rho U V_x\}^* V_x + (M/\rho c)P^* P] \tag{30a}$$

$$I_{y1} = \tfrac{1}{2}\mathrm{Re}[\{P+\rho U V_x\}^* V_y] \tag{30b}$$

$$I_{z1} = \tfrac{1}{2}\mathrm{Re}[\{P+\rho U V_x\}^* V_z] \tag{30c}$$

$$I_{x2} = \tfrac{1}{2}\mathrm{Re}[P^* V_x + (M/2\rho c)P^* P + \tfrac{1}{2}\rho U(V_x^* V_x + V_y^* V_y + V_z^* V_z)] \tag{31a}$$

$$I_{y2} = \tfrac{1}{2}\mathrm{Re}[P^* V_y] \tag{31b}$$

$$I_{z2} = \tfrac{1}{2}\mathrm{Re}[P^* V_z] \tag{31c}$$

In the case of a line-excited plate without flow, these expressions reduce to those used by Spicer [8].

5. FAR-FIELD RADIATED SOUND PRESSURE

The far-field sound pressure can be evaluated for both point- and line-force excitation using the method of stationary phase, which is described in some detail, for the case of point-force excitation, in Appendix A.

(a) Point-force Excitation

The far-field pressure in the case of point-force excitation is best evaluated using a non-standard spherical co-ordinate system identical to that used by Leppington & Levine [20] to calculate the far-field pressure of a circular piston set in an infinite rigid baffle. The co-ordinate system is defined by

$$x = R\cdot\cos\theta, \quad y = R\cdot\sin\theta\cdot\sin\psi, \quad z = R\cdot\sin\theta\cdot\cos\psi \tag{32}$$

and illustrated in Figure 2(a). The stationary phase point

(α_0, β_0) is given by

$$\alpha_0 = [k/(1-M^2)][-M + \cos\theta \,/\, \sqrt{\{h(M,\theta)\}}] \tag{33}$$

$$\beta_0 = k\cdot\sin\theta\cdot\sin\psi \,/\, \sqrt{\{h(M,\theta)\}} \tag{34}$$

where

$$h(M,\theta) = 1 - M^2\sin^2\theta \tag{35}$$

The resulting expression for the far-field pressure is

$$P(R,\theta,\psi) = \frac{F_0\left[\frac{-ik}{2\pi R}\right](1-\alpha_0 M/k)^2\left[\frac{\sin\theta\cdot\cos\psi}{h(M,\theta)}\right]\exp\{iR\cdot g(k,M,\theta)\}}{(1-\alpha_0 M/k)^2 - \left[\frac{ik\cdot\sin\theta\cdot\cos\psi}{\mu\cdot\sqrt{\{h(M,\theta)\}}}\right]\{1-(\alpha_0^2+\beta_0^2)^2/k_p^4\}} \tag{36}$$

where

$$g(k,M,\theta) = [k/(1-M^2)][-M\cdot\cos\theta + \sqrt{(1-M^2\sin^2\theta)}] \tag{37}$$

The expression for $g(k,M,\theta)$ is identical to that obtained by Leppington & Levine for the piston problem. It can be shown that equation (36) reduces to the well-known classical result in the no-flow case. Equations (32) to (37) are expressed in terms of the traditional spherical co-ordinate system (Figure 2(b)) in Appendix B.

(b) Line-force Excitation

A cylindrical co-ordinate system is used defined by

$$x = R\cdot\cos\theta, \quad y = R\cdot\sin\theta \tag{38}$$

and illustrated in Figure 2(c). The stationary phase point is given by

$$\alpha_0 = [k/(1-M^2)][-M + \cos\theta \,/\, \sqrt{\{h(M,\theta)\}}] \tag{39}$$

where $h(M,\theta)$ is given by equation (35). Equation (39) gives an expression for α_0 which is identical to that in the case of point-force excitation, equation (33). The far-field pressure is given by

$$P(R,\theta) = \frac{F_0\left[\frac{-ik}{2\pi R}\right]^{1/2}(1-\alpha_0 M/k)^2\left[\frac{\sin\theta}{h(M,\theta)^{3/4}}\right]\exp\{iR\cdot g(k,M,\theta)\}}{(1-\alpha_0 M/k)^2 - \left[\frac{ik\cdot\sin\theta}{\mu\cdot\sqrt{\{h(M,\theta)\}}}\right]\{1-\alpha_0^4/k_p^4\}} \qquad (40)$$

where $g(k,M,\theta)$ is given by equation (37).

Inspection of equations (36) and (40) reveals that the expressions for the far-field pressure can vanish if $\alpha_0=k/M$, but this is only true if $M=1$. For the range of Mach numbers encountered in water-loaded plates the theory indicates that the flow has only a very small effect and this is borne out in the numerical calculations described in Section 7.3.

6. DISCUSSION OF STABILITY

(a) Steady-state Approach

It is instructive at this stage to apply the results of Benjamin [13,14] and Landahl [15] to the stability of a line-excited plate. Their results are obtained for the general problem of inviscid fluid flow over a flexible solid plane boundary. Provision is made for including damping in the solid and the effect of a thin boundary layer in the fluid. In the absence of a boundary layer and for an undamped plate, the equation for the phase speed can be expressed in the present notation as

$$(U-c_p)^2 = (\rho_S h\alpha/\rho)(c_0^2-c_p^2) \qquad (41)$$

where c_p is the phase speed of free waves in the coupled plate-fluid system and c_0 the speed of in vacuo free waves in the plate, given by

$$c_0 = \alpha\cdot\sqrt{(D/\rho_S h)}$$

Writing

$$\zeta = \rho_S h\alpha/\rho$$

equation (41) can be expressed as a quadratic in c_0 which can be solved to give c_0 as a function of ζ and c_0 (which are both functions of α), viz.

$$c_p = [1/(\zeta+1)][U + \sqrt{\{\zeta(\zeta+1)c_0^2 - \zeta U^2\}}] \qquad (42)$$

For a fixed positive value of α, there are three distinct possibilities, which Benjamin and Landahl interpret as follows:

(i) $U^2 < \zeta c_0^2$, which gives one positive and one negative root. The negative root corresponds to a wave propagating in the opposite direction to the flow. Benjamin [14] showed that this wave decays if damping is present in the plate. The wave with positive c_p also propagates without damping in the plate, but it may be destabilized in the presence of a boundary layer. This wave corresponds to a class B instability, as mentioned in the Introduction.

(ii) $\zeta c_0^2 < U^2 < (\zeta+1)c_0^2$, which gives two positive roots, one less than U and the other greater than U. The faster wave has properties similar to the wave with positive c_p in case (i). In a uniform flow, the slower wave is destabilized by damping in the plate, corresponding to a class A instability. The transition between cases (i) and (ii), i.e.

$$U^2 = \zeta c_0^2 \quad \text{or} \quad c_p = 0$$

can be expressed as

$$\rho U^2 = D\alpha^3 \qquad .$$

This corresponds to the condition known as "static divergence" in studies of panel flutter. The hydrodynamic pressure is just sufficient to maintain a stationary wave against the resilient restoring forces. For an infinite plate, this condition occurs at zero frequency giving an infinite wavelength, as mentioned by Dowell [21]. Dowell pointed out that no physical significance can be attached to this result for an infinite plate, but for a plate of finite width or an infinite plate resting on an elastic foundation, both the critical wavelength and flutter velocity become finite.

(iii) $U^2 > (\zeta+1)c_0^2$, which gives two complex values of c_p, one of which has a positive imaginary part and thus represents a propagating wave, the amplitude of which grows exponentially with time. This is a Class C instability.

The above approach to stability is compared with that using the causal approach (see Section 6(b) below) in Section 8.

(b) Causal Approach

In Sections 2 to 5 it is assumed that the excitation $F_0\exp(-i\omega_0 t)$ exists for all time t. In practice, however, the excitation may be switched on at some instant, say $t=0$, and steadily maintained thereafter. If this is the case, then there are three possibilities for the response at any point of the system after a long time has elapsed. The amplitude may either (i) settle down to the steady-state value, (ii) settle down to a different steady-state value but increase exponentially with distance, or (iii) grow exponentially with time at every point of the system. Case (ii) is termed a convective instability and case (iii) an absolute instability (Melcher [18]).

This form of excitation can be represented mathematically by a Laplace-Fourier transform. To simplify the analysis, the specific example of the displacement of a line-excited plate is discussed. However, the technique described here can be applied to the plate displacement, the acoustic pressure and the acoustic particle velocities of both point- and line-excited plates.

Suppose that the plate displacement $w(x,t)$ can be expressed in terms of a complex time-dependent amplitude

$$w(x,t) = \mathrm{Re}[W(x,t)]$$

Then the Laplace-Fourier representation of W is

$$W(x,t) = (1/2\pi) \int_{-\infty+i\sigma}^{\infty+i\sigma} \tilde{W}(x,\omega)\, \exp(-i\omega t)\, d\omega \qquad (43)$$

$$\tilde{W}(x,\omega) = (1/2\pi) \int_{-\infty}^{\infty} \bar{W}(\alpha,\omega)\, \exp(i\alpha x)\, d\alpha \qquad (44)$$

where

$$\bar{W}(\alpha,\omega) = iF_0/\{(\omega-\omega_0)Z(\alpha,\omega)\} \qquad (45)$$

and σ is a positive constant such that the contour $\mathrm{Im}(\omega)=\sigma$ lies above any singularities of $\tilde{W}(x,\omega)$. This ensures that causality is satisfied, i.e. that the response of the system is zero for $t<0$. In equation (45), $Z(\alpha,\omega)$ is given by equation (21) with ω_0 replaced by ω.

Provided that the radiation condition is satisfied along the

real axis, the integrand of equation (44) can be analytically continued into the complex α-plane. However, the integrand has branch points at

$$\alpha = \alpha^- = -k/(1-M), \qquad \alpha = \alpha^+ = k/(1+M)$$

corresponding to $\gamma=0$. For $\sigma>0$, these branch points are off the real α-axis and in opposite half-planes. The associated branch cut must not cross the real α-axis and must therefore go to infinity, the cut from α^+ going to $+\infty$ and that from α^- going to $-\infty$. Apart from this restriction, the choice of branch cuts is arbitrary. For simplicity, the branch cuts used in all the numerical work are defined by $\mathrm{Im}[\gamma]=0$, as a result of which

$$\gamma = \sqrt{\{k^2(1-\alpha M/k)^2 - \alpha^2\}}, \qquad \mathrm{Im}[\gamma]>0 \tag{46}$$

everywhere, except on the branch cuts.

The Fourier integral (44) can be evaluated by suitably closing the contour and applying Cauchy's theorem. Figure 3 illustrates the case when $x>0$, requiring the contour to be closed in the upper half-plane. For $x<0$, the contour is closed in the lower half-plane. This convention ensures that, as $\mathrm{Im}[\alpha]$ tends to infinity, the term $\exp(i\alpha x)$ in the integrand remains finite. In Figure 3, let α_j^+ $(j=1,3)$ represent all the singularities of the integrand in the upper half-plane and α_j^- $(j=1,3)$ those in the lower half-plane. If σ is large enough, then all the poles are well clear of the real axis. The contours C_1 and C_2 are circular arcs of large radius and, provided that all singularities in the upper half-plane lie inside the contour, the contributions from C_1 and C_2 tend to zero as the radius tends to infinity. The integrals along B_1, B_2 and B_3 are branch cut integrals which are discussed later in the Section. The integral (44) can be expressed using Cauchy's theorem as the sum of residues and branch cut integrals, in the form

$$\tilde{W}(x,\omega) = \pm \sum_{j=1}^{3} -F_0 \exp(i\alpha_j^{\pm}x)/\{(\omega-\omega_0)Z'(\alpha_j^{\pm},\omega)\} + \text{branch cut integrals} \tag{47}$$

where the + sign corresponds to positive values of x and the - sign to negative values of x.

The plate response is given by using equation (43) to integrate $\tilde{W}(x,\omega)$ over the Laplace contour. For $t<0$, the contour must be closed as in Figure 4(a) to be consistent with causality.

For $t>0$, any numerical scheme to evaluate the integral (43) would eventually become unstable at large t because the term $\exp(-i\omega t)$ in the integrand tends to infinity as $t\to\infty$. For this reason and also to be able to provide a physical interpretation of the response when t is large and positive, it is necessary to move the Laplace contour down to the real axis, i.e. to let σ tend to zero. If there are no singularities of $\tilde{W}(x,\omega)$, apart from that at $\omega=\omega_0$, then the Laplace contour for large t can be moved so that it lies just below the real axis, indented around $\omega=\omega_0$ and closed in the lower half-plane, as in Figure 4(b). The plate response can now be expressed as the sum of modes and branch cut integrals

$$W(x,t) = \sum_{j=1}^{3} W_j^{\pm} \exp(-\alpha_j^{\pm} x)\exp(-i\omega_0 t) + \text{branch cut integrals} \quad (48)$$

where

$$W_j^{\pm} = \pm\{-F_0/Z'(\alpha_j^{\pm},\omega_0)\}$$

In order to ascertain whether or not any physical significance can be attached to each mode of the plate response, it is necessary to use the root locus technique described by Melcher [18]. First consider when there are no singularities of $\tilde{W}(x,\omega)$ in the upper-half ω-plane, and ignore, for the moment, the contribution of the branch cut integrals. For a given ω_0, the loci of the roots $\alpha_j^{\pm}$ (which are functions of ω) are plotted for values of $\omega=\omega_0+i\sigma$ as σ varies from $+\infty$ to 0. As the Laplace contour is moved down to the real ω-axis, the poles enclosed by the Fourier contour also move and it may be necessary to deform the Fourier contour so that it always includes the same poles of $\bar{W}(\alpha,\omega)$. There are six basic possibilities, illustrated in Figure 5(a). The shaded circles in this Figure denote points where the loci terminate, corresponding to $\omega=\omega_0$.

Suppose that a locus comes from infinity in the upper half α-plane to a value above the real axis, say $\alpha_r+i\alpha_i$ with $\alpha_i>0$ (case (i) in Figure 5(a)). The response of this mode is nonzero only for $x>0$, in which case

$$W(x,t) = W_1\exp\{(i\alpha_r-\alpha_i)x\}\exp(-i\omega_0 t)$$

which gives a decaying or "evanescent" wave. If the locus terminates on the real axis (case (ii)), the response for $x>0$ becomes

$$W(x,t) = W_2 \exp(i\alpha_r x)\exp(-i\omega_0 t)$$

which represents a travelling, non-decaying wave. Since the locus comes from above the real axis, the Fourier contour must be indented below the pole. The wave is travelling in the x-increasing direction, (i.e. outwards from the excitation) if α_r is positive and in the x-decreasing direction (i.e. inwards from infinity) if α_r is negative. If the locus crosses the real α-axis (case (iii)), the Fourier contour can no longer be taken along the real axis but must be deformed around the pole. If the pole is at $\alpha=\alpha_r-i\alpha_i$, where $\alpha_i>0$, then the response for $x>0$ is

$$W(x,t) = W_3 \exp\{(i\alpha_r+\alpha_i)x\}\exp(-i\omega_0 t)$$

which for positive α_r denotes a wave propagating in the x-increasing direction and increasing exponentially in amplitude with distance. This is usually termed a "convective instability". Cases (iv) to (vi) are identical to cases (i) to (iii) respectively, except that the responses are non-zero only for $x<0$.

Suppose there are zeros of $Z'(\alpha_j,\omega)$ in the ω-plane, where α_j is one of the the roots of the dispersion relation $Z(\alpha,\omega)=0$. Then these must be identified as possible singularities of $\tilde{W}(x,\omega)$. Melcher [18] shows that a singularity of $\tilde{W}(x,\omega)$ in the ω-plane is the result of the coalescence of a pair of poles in the α-plane. He also shows that there are four distinct possibilities here, illustrated as Figure 5(b). Suppose that both loci come from either above or below the real α-axis and coalesce before reaching the axis (case (i)) or on the axis (cases (ii) and (iii)). Melcher points out that the terms of $\tilde{W}(x,\omega)$ corresponding to each pole contain a singularity, but when they are combined the singularities are not present. Hence the only singularity in the ω-plane is at $\omega=\omega_0$ and the Laplace integral can be evaluated giving equation (48). The physical significance of the resulting modes then depends on where the loci terminate, as shown in Figure 5(b). In case (iv), a locus coming from above the α-axis coalesces with one coming from below. In this case, Melcher showed that the Fourier contour can no longer be distorted to include the same poles but will always include one or the other when closed in the upper or lower half α-plane. In the ω-plane there is a branch pole in the upper half-plane, at $\omega=\omega_s$, and when the Laplace contour is deformed around this, there is always a contribution $\exp(\omega_s t)$ to the response, with $\omega_s>0$. Hence the response grows exponentially with time at a fixed location x. This is termed an "absolute instability", which occurs whatever the value of ω_0.

It is now necessary to discuss the branch cut integrals. In

the absence of flow, Strawderman et al. [6] show that the contribution arising from the circular contour B_2 around the branch point is zero, and that, provided the branch cuts are well away from any singularities of the integrand, the integrals along B_1 and B_3 contribute only to the near field because the integrands are bounded. It can be shown, by a simple linear mapping, that the integrals with flow can be converted to the same form as those without flow, and hence that the above results also apply in the presence of flow. Crighton [7] has pointed out, for the case of an undamped plate without flow, that it is only those poles that exist for all suitable choice of branch cuts which have any physical significance at large x. The remaining poles contribute only to the near field and their contributions must always be combined with those from the branch cut integrals.

As already mentioned in this Section, if σ is large enough, all the poles of the integrand of equation (44) are well away from the real axis. A consequence of this is that the location of the poles depends on the particular choice of branch cuts and that no pole exists for all possible choices of branch cuts. It also means that, as σ varies, a root locus corresponding to the movement of a particular pole may cross a branch cut and "disappear", or vice versa. At $\sigma=0$, the poles corresponding to evanescent waves also depend on the choice of branch cuts. The contribution to the response arising from these poles can therefore have no physical significance in isolation, but must be combined with the branch cut integrals. A free-wave pole (i.e. one on the real axis for $\sigma=0$) always exists for all possible choices of branch cut and therefore has physical significance. A pole corresponding to a convective instability crosses the real axis at some positive value of σ and always exists in a neighbourhood of the real axis. Furthermore, if coalescing poles in the α-plane corresponding to a singularity in the upper-half ω-plane exist, they do so for all possible choices of branch cut.

To summarize, provided that there are no singularities of $\tilde{W}(x,\omega)$ in the ω-plane, the root locus technique can be used to determine the physical significance of a wave having complex values of α for real ω. The modes of the response can be either non-decaying travelling waves or convectively amplifying waves. If a singularity exists anywhere in the upper half ω-plane as a result of coalescing poles whose loci in the α-plane come from opposite half-planes, then the system has an absolute instability and the response grows with time at a fixed location. In practice, this is usually damped by some nonlinear mechanism or a factor not taken into account in the current theory. A necessary condition for instability (absolute or convective) is that a locus in the α-plane crosses the real axis. This implies that for some real wavenumber α, the dispersion relation must have a root ω with a positive imaginary part, the criterion used by Benjamin [13,14], Landahl [15] and Miles [16] to determine instability.

7. NUMERICAL RESULTS

All the numerical results presented in this section are for an infinite steel plate of thickness 5 cm, with $E=19{\cdot}5\times10^{10}$ N/m^2, $\nu=0{\cdot}29$ and $\rho_S=7700$ kg/m^3. The plate is immersed in water of density 1000 kg/m^3 and sound speed 1500 m/s. The quantity F_0 is 1N in the case of point-force excitation and 1 N/m in the case of line-force excitation. Plate damping when used is represented by a complex Young's modulus $E=E(1-i\eta)$, where η is a hysteretic loss factor. Two flow speeds are considered, $U=7{\cdot}5$ and $22{\cdot}5$ m/s (15 and 45 knots), equivalent to Mach numbers of $0{\cdot}005$ and $0{\cdot}015$ respectively. Most of the numerical results are limited to the case of line-excited plates, but the far-field pressure computations are for both point- and line-excited plates.

(a) Dispersion Plots

For an undamped line-excited plate, the real roots of the dispersion relation $Z(\omega_0,\alpha)=0$ (where $Z(\omega_0,\alpha)$ is defined by equation (21)) determine the wave numbers α corresponding to free waves propagating along the plate at a given frequency ω_0. Positive values of α correspond to waves propagating in the x-increasing direction and negative values to waves propagating in the x-decreasing direction.

Figure 6 shows a plot of wavenumber α against frequency f $(=\omega_0/2\pi)$ for a line-excited plate with a $7{\cdot}5$ m/s flow, which is compared with the corresponding plot in the absence of flow. At low frequencies the flow has a significant effect on wavenumber at a given frequency. Further results not presented here indicate that with increasing frequency the values of α with flow approach those without flow. At frequencies above coincidence (approximately 5 kHz), values of α with and without flow are almost identical. In the case with flow, at frequencies between f_L (approximately $0{\cdot}109$ Hz) and f_U (approximately $0{\cdot}121$ Hz), the number of positive roots of the dispersion relation changes from one to three. At frequencies f_L and f_U, two of these positive roots coalesce. This effect is discussed in Section 7(d) below. At a frequency f_C of approximately $0{\cdot}112$ Hz, the curve with flow for positive values of α has a local minimum value.

Figure 7 shows plots of phase velocity ω_0/α and group velocity $\partial\omega_0/\partial\alpha$ against frequency at a flow speed of $7{\cdot}5$ m/s. At frequencies below f_L ($0{\cdot}109$ Hz), the positive value of phase velocity is less than the flow speed while, at frequencies above f_U ($0{\cdot}121$ Hz), it is greater than the flow speed. At frequencies above coincidence, further numerical results not presented here indicate that the phase speed of the upstream wave tends to c-U and that of the downstream wave to c+U. At the frequency f_C ($0{\cdot}112$ Hz), corresponding to the local minimum in the wavenumber-

frequency curve (Figure 6), the group velocity has a singularity. At low frequencies, there are two negative values of group velocity which, as the frequency tends to zero, both tend to the same limiting value, approximately $(-3/2)U$. This limiting value can also be obtained from the dispersion relation by expressing it as a function of α and ω_0 and taking the limit as $\omega_0 \to 0$ of

$$-(\partial Z/\partial \alpha)/(\partial Z/\partial \omega_0)$$

The result is $(-3/2)U$ multiplied by a negligibly small Mach number correction arising from the compressibility of the fluid. If the plate is substituted by a membrane, with $D\alpha^4$ in the dispersion relation replaced by $T\alpha^2$, where T is the tension in the membrane, then the limiting group velocity at zero frequency becomes $(-1/2)U$ with the same Mach number correction. This effect is discussed below in Section 8. This corresponds to static divergence as mentioned in Section 6(a).

Figure 8 shows a plot of wavenumber against frequency at a flow speed of 22·5 m/s, which is also compared with the corresponding no-flow plot. The dispersion relation only has one real positive root α over the whole frequency range, which implies that there are no real values of α and ω_0 for which $Z'(\alpha,\omega_0)=0$, and hence no coalescing poles on the real α-axis. Figure 9 shows plots of phase and group velocities at the same flow speed. There is a singularity in the group velocity and the limiting value of group velocity at zero frequency is $(-3/2)U$, the same result as with a flow speed of 7·5 m/s.

It is possible to find all the complex roots α of the dispersion relation $Z(\alpha,\omega)=0$ corresponding to real values of ω. However, the number and location of the complex roots depends on the choice of branch cuts, and therefore (according to Crighton [7]), no physical significance can be attached to any of the complex roots. Another approach is to find the real and complex roots ω corresponding to real values of α, since this determines free waves of the form $\exp(i\alpha x - i\omega t)$ with α real. If $\mathrm{Im}[\omega]>0$, this indicates a wave the amplitude of which grows with time. Without loss of generality, $\mathrm{Re}[\omega]$ can be restricted to positive values, which gives, as before, positive values of α corresponding to waves propagating in the x-increasing direction, and negative values to waves propagating in the x-decreasing direction.

Figure 10 shows wavenumber plotted against the real and imaginary parts of frequency, at a flow speed of 7·5 m/s. At values of α greater than about 0·1 or less than about -0·29, the dispersion relation gives only real values of ω corresponding to propagating waves identical to those plotted in Figure 8. At small positive values of α up to about 0·1, the

dispersion relation gives a pair of complex conjugate roots ω. The root with positive imaginary part corresponds to an amplifying wave propagating in the x-increasing direction. Figure 11 is similar to Figure 10, but is at a flow speed of 22·5 m/s. This also gives an amplifying wave propagating in the x-increasing direction for positive values α up to about 0·24. It is possible to deduce from Figures 10 and 11, using arguments put forward in Section 6, that an instability of some sort (convective or absolute) exists at both flow speeds. However, it is not possible to make any further deduction as to the exact nature of the instability by using the information supplied by Figures 6 to 11 alone.

(b) Far-field Pressure Computations Using Steady-state Approach

Some numerical comparisons have been made of far-field pressure with and without flow for damped point- and line-excited plates with a loss factor η=0·02 over a frequency range of 0·01 Hz to 10 kHz. Corresponding results with and without flow are identical to within 0·1 dB in amplitude and 2° in phase at all frequencies up to 1 kHz (i.e at frequencies below coincidence). Tables I and II illustrate the differences with and without flow at 10 kHz (i.e. above coincidence) for point- and line-force excitation respectively. The far-field sound pressures are calculated at a nominal radius of 1 m for various values of θ (with ψ=0 in the case of point-force excitation) and the amplitudes are expressed in dB re 1 μPa. The comparisons show that the main effect of the flow is to slightly change the direction of the coincidence lobes, while not changing the peak amplitude. In the case of point-force excitation, results with ψ=90° not presented here show much less of a flow effect. This indicates that the predominant flow effect is felt directly upstream and downstream of the force rather than in any other direction.

(c) Intensity Vector Plots Using Steady-state Approach

Intensity vectors have been calculated numerically for a line-excited damped plate, by adapting the computer programs written by Spicer [8] to incorporate the effect of flow. Both formulations of acoustic intensity (equations (30) and (31)) have been incorporated into the new programs. Figures 12 to 15 illustrate the variation with frequency of intensity vectors along the plate surface. In these Figures, the length of each vector is proportional to the square root of its magnitude. Each row of intensity vectors was computed separately and each vector in a particular row was normalised with respect to the maximum value in that row. Figure 12 shows intensity vectors according to formulation 1, at a flow speed of 7·5 m/s. At frequencies above

and below 0·12 Hz, the free wave propagating away from the force in the x-increasing direction corresponds with the positive wavenumber and that in the x-decreasing direction with the negative wavenumber. At intermediate frequencies, the predominant acoustic energy flow is aligned with the fluid flow. Figure 13 shows results using formulation 2 at some of the selected frequencies. There are slight differences between the two sets of results. Downstream of the excitation, both formulations give similar results, but upstream, at frequencies below 0·12 Hz, the two sets of results are approximately 180° out of phase. Figure 14 compares results with and without flow. The flow is seen to have an effect only at very low frequencies. In Figure 15, results using formulation 1 at a flow speed of 22·5 m/s show similar effects to those in Figure 12. These results are discussed further in Section 8.

According to equations (8), (13), (14) and (15), at a frequency at which $(1-\alpha M/k)$ vanishes, then the contribution to the acoustic intensity vector from the corresponding free wave pole α also vanishes. This frequency corresponds to that where the phase speed equals the flow speed and it is given by

$$\omega_0 = U^2\sqrt{(\rho_S h/D)}$$

corresponding to approximately 0·12 Hz and 1·06 Hz at flow speeds of 7·5 and 22·5 m/s respectively. At 7·5 m/s (Figures 12 and 13), the acoustic intensity at 0·12 Hz does not decay rapidly downstream of the excitation, whereas it does so at 0·14 Hz. At 22·5 m/s (Figure 15), the downstream acoustic intensity decays rapidly at 1·0 Hz. At both flow speeds, the rate of decay falls off as the frequency is increased.

(d) Numerical Determination of Stability Characteristics Using Causal Approach

In order to use the root locus technique to determine stability, the complex roots α of the dispersion relation for a real or complex frequency ω need to be found. The numerical procedure used to do this was to apply Newton's method in the complex plane starting from each point on a grid. Numerical tests for convergence, divergence and finding the same root more than once were incorporated into the method. At low frequencies, the compressibility of the fluid can be neglected and the dispersion relation reduces to a polynomial, in which case standard numerical techniques are available for extraction of the roots. Comparison of both methods yielded almost identical results up to at least 10 Hz.

Figure 16 shows root loci diagrams at a flow speed of 7·5 m/s for an undamped line-excited plate. The loci, plotted for

various values of ω_0, represent the movement of the roots α of the dispersion relation

$$Z(\omega,\alpha) = 0 , \quad \omega = \omega_0 + i\sigma$$

as σ varies from a large positive value to zero. On Figure 16, the circles represent points where $\sigma=0$. All the loci labelled 1 correspond to a frequency $\omega_0/2\pi$ of 0·04 Hz. The loci labelled 1a and 1b terminate on the real α-axis and, using the results of Section 6(b), represent outgoing and incoming waves respectively in the region $x<0$. The locus labelled 1c crosses the real α-axis and terminates in the lower half-plane. This represents an outgoing wave in the region $x>0$, the amplitude of which increases exponentially with distance (i.e. a convective instability). The locus labelled 1d terminates in the upper half-plane. If σ is greater than a certain value, then this locus crosses the branch cut (which at low flow speeds and relatively small values of σ is almost coincident with the positive imaginary axis) and "disappears". The locus marked 1e only exists for relatively large values of σ. As the loci 1d and 1e do not exist in some neighbourhood of the real α-axis, then (as mentioned in Section 6(b)), they are of no physical significance in isolation, but the contribution from these poles must be combined with the branch cut integrals.

At a frequency of 0·08 Hz, the loci (labelled 2a-2e in Figure 16) show the same behaviour as those at 0·04 Hz. At 0·12 Hz, there are four loci (labelled 3a-3d) which terminate on the real axis. Reference to Figure 6 indicates that, at this frequency, the dispersion relation has four real roots. There are two propagating waves, one incoming and one outgoing, in $x<0$ and two outgoing waves in $x>0$. At 0·16 Hz, two of the loci (4a and 4c) terminate on the real axis and hence represent propagating outgoing waves, one in $x>0$ and one in $x<0$. The other two loci (4b and 4d) represent evanescent waves and are of no physical significance in isolation. The loci at 0·2 Hz show the same behaviour as those at 0·16 Hz.

The above results indicate that there are three distinct frequency bands where the results have different interpretations. The boundaries between these bands are the frequencies f_L and f_U (approximately 0·109 and 0·121 Hz respectively) mentioned in Section 7(a) and Figure 6, where there are coalescing poles on the real α-axis. Melcher [18] shows that neither case of coalescing poles corresponds to an absolute instability. Further numerical work not presented here indicates that there are no other cases of coalescing poles in the α-plane. Although there are examples in Figure 16 of loci at the same value of ω_0 which intersect, the points of intersection correspond to different values of σ and so they are not examples of coalescing poles. Hence there is no absolute instability and the interpretation of

the results in the two previous paragraphs is valid. This interpretation is compared with that using the Benjamin-Landahl approach to stability in Section 8.

The numerical results presented in Figure 16 were repeated with plate damping. The plate loss factor chosen was 0·2, rather higher than encountered in practice in order to exaggerate the effects of damping for clarity. The results are shown in Figure 17. The loci corresponding to propagating waves with negative α move downwards, i.e. away from the axis and hence represent waves propagating away from the excitation in the region $x<0$ and slowly decaying to infinity. At frequencies below f_L (0·109 Hz), the locus corresponding to the incoming wave from infinity in $x<0$ now crosses the real axis, which suggests that this wave is destabilized by plate damping. Further numerical work is necessary to clarify and quantify this effect. At frequencies above f_U (0·121 Hz), both the loci corresponding to propagating waves move away from the real axis and hence both waves slowly decay to infinity. In the intermediate region corresponding to four propagating waves, all the loci move away from the axis.

Figure 18 is similar to Figure 16 but is at a flow speed of 22·5 m/s. At a frequency of between 0·8 and 0·85 Hz, the diagram shows coalescing poles at a point not on the real α-axis, one coming from above and one from below. As mentioned in Section 6, this is indicative of an absolute instability where the linear theory predicts that the response at every point of the system grows exponentially with time. Further numerical results not presented here suggest that plate damping does not remove the singularity, but merely changes its location slightly.

8. DISCUSSION OF RESULTS

Comparison of the causal approach and the Benjamin-Landahl approach to stability indicates that provided the causal approach does not give an absolute instability, both methods give the same interpretation of the various free waves. The comparison is illustrated in Figure 19. It should be noted that where a convectively unstable wave exists it will dominate the response in the region $x<0$ or $x>0$. The amplitude of the disturbance (assumed by the linear theory to be infinitesimal) increases with distance until it can no longer be assumed to be infinitesimal, when linear theory breaks down and the disturbance is damped by a non-linear mechanism.

The next question to be resolved is the interpretation of the intensity vector plots in the light of the stability results. The intensity vector plots were obtained by integrating numerically along the real α-axis. With damping the free wave poles in the α-plane move off the real axis, and integrating along the real axis implies, according to Crighton [7], that the

free wave poles always represent outgoing waves, as is the case for a line-excited plate without flow. In order to satisfy causality in systems with a convective instability, the Fourier contour (in the α-plane) must be deformed around the pole giving rise to the instability, and the plate response, acoustic pressure and acoustic particle velocities must be evaluated along the deformed contour. Hence further numerical work is necessary to quantify the effect of convective instabilities on far-field sound pressure and acoustic intensity. In addition, care is required in attaching any physical significance to the intensity vector plots (Figures 12 to 15) at combinations of flow speed and frequency giving rise to a convective instability.

According to Brazier-Smith & Scott [19], the causal approach to stability predicts a critical flow speed above which the line-excited plate with flow is absolutely unstable. The flow speed is given by

$$U = 0{\cdot}074\rho\sqrt{(D/\rho_S{}^3h^3)}$$

which for a steel plate in water reduces to a flow speed of approximately 15 m/s (30 knots) or $M=0{\cdot}01$. This speed can be determined by obtaining the dispersion relation $Z(\omega,\alpha)=0$ for incompressible flow and considering when

$$\partial Z/\partial\alpha = \partial^2 Z/\partial\alpha^2 = 0$$

i.e. it is equivalent to the case where there are three coalescing poles on the real α-axis. One consequence of this onset of absolute instability is that at flow speeds above the critical speed, the pressure and acoustic particle velocities cannot be determined using the current linear theory. It is well known that in a finite system with flow, if a resonant mode of the system is excited at a particular flow speed the level of radiated sound increases dramatically. This may also be the case in situations where linear theory predicts absolute instability of an infinite system. Hence care is required in interpreting any numerical results at the higher flow speed.

9. CONCLUSIONS AND SUGGESTIONS FOR FURTHER RESEARCH

Expressions have been obtained for the plate response, acoustic pressure and acoustic intensity vectors of point- and line-excited infinite fluid-loaded plates in the presence of uniform inviscid flow. The expressions were obtained from the steady-state equations of motion in the form of Fourier integrals along the real wavenumber axis. Two expressions have been

extracted from the literature for the acoustic intensity vector in the presence of a uniform flow. For the particular case of steel plates in water at flow speeds of less than 15 m/s (30 knots), the flow generally has very little effect on radiated sound pressure and the response of a line-excited plate consists of waves propagating away from the excitation. At very low frequencies, however, the downstream response of a line-excited damped or undamped plate is convectively unstable and one component of the upstream response is an incoming wave from infinity which is apparently destabilized by damping. These results are consistent with those obtained by examination of the dispersion relation to find free waves with real wavenumbers corresponding to complex values of frequency with positive imaginary parts. At flow speeds above 15 m/s, a causal approach to stability indicates that the coupled system is absolutely unstable and linear theory breaks down.

There are several areas in which the work can be extended. Although the interesting physical effects occur at extremely low frequencies for steel plates in water, for other materials, e.g. soft and hard rubber, the various critical frequencies and the critical flow speed are generally different, and the critical frequencies may well be much higher, and hence of more practical significance. The theory can also be extended to consider finite plates or infinite strips, the stability of which has been tackled using the Benjamin-Landahl approach but not the causal approach. There has been much intramural and extramural work done by AMTE and contractors on sound radiation and wave propagation in more complex fluid-loaded structures such as stiffened plates, infinite cylinders with internal and external fluid loading, and layered media. The effect of flow on these systems needs to be studied and quantified.

One limitation in the present work is that the mean flow is assumed to be uniform. In practice there is a thin boundary layer next to the plate surface in which the mean flow velocity changes from zero at the undisturbed plate surface to the free stream value. In general this boundary layer is turbulent which means that the flow itself is an additional excitation source. The effects of laminar and turbulent boundary layers on plates and more complex dynamical systems need to be examined and quantified. A number of investigations have already been undertaken on this topic. Benjamin [14] has incorporated a representation of a thin laminar boundary layer with zero pressure gradient in the form of a small correction to the surface pressure. Ffowcs-Williams & Purshouse [22] have used a vortex sheet model of a boundary layer in the problem of a baffled piston vibrating beneath a boundary layer. They showed that whereas a uniform flow at low speed reduces the resonant frequency of the piston and above a certain speed induces instability and flutter, the vortex sheet model predicts that in many cases the effect of the flow is to increase the resonant frequency without any flutter. These latter predictions agree

with experiment.

Although there has been much theoretical work done on the stability of flow over surfaces, there has been relatively little corresponding laboratory experimental work. The experiments of Gupta et al. [17] are described in the Introduction. Hansen et al. [23] have conducted stability experiments on a finite plate and rotating disc. They observed three different types of surface waves on the plate and two on the disc. One of the plate waves was attributed to an irregularity in the plate geometry, but all the other waves could be predicted theoretically. The propagation velocities for all the disturbances were substantially below the free-stream fluid velocity.

Because of the low wavenumbers and hence large wavelengths involved even with very thin steel plates, experiments to test the present theory using steel plates in water would be impractical. However there may be other materials with substantially different physical properties which could be used in water-tunnel tests.

D.J.Atkins (HSO)

Manuscript completed August 1982

REFERENCES

1. GUTIN,L.Y., Sound radiation from an infinite plate excited by a normal point force, Sov. Phys.-Acoust. 10(4)369-371(1965)

2. FEIT,D., Pressure radiated by a point-excited elastic plate, J. Acoust. Soc. Am. 40(6)1489-1494(1966)

3. JUNGER,M.C. & FEIT,D., Sound structures and their interaction, MIT Press(1972)

4. STUART,A.D., Acoustic radiation from submerged plates. I. Influence of leaky wave poles, J. Acoust. Soc. Am. 59(5)1160-1169(1979)

5. STUART,A.D., Acoustic radiation from submerged plates. II. Radiated power and damping, J. Acoust. Soc. Am. 59(5)1170-1174(1979)

6. STRAWDERMAN,W.A., et al., The real roots of the fluid-loaded plate, J. Acoust. Soc. Am. 66(2)579-585(1979)

7. CRIGHTON,D.G., The free and forced waves on a fluid-loaded elastic plate, J. Sound Vibr. 63(2)225-235(1979)

8. SPICER,W.J., Acoustic intensity vectors from an infinite plate with line attachments, AMTE(N)TM81086(1981)

9. RYSHOV,O.S. & SHEFTER,G.M., On the energy of acoustic waves propagating in moving media, J. Appl. Math. & Mech. 26(5)1293-1309(1962)

10. MORFEY,C.L., Acoustic energy in non-uniform flows, J. Sound Vibr. 14(2)159-170(1971)

11. CANDEL,S.M., Acoustic conservation principles and an application to plane and modal propagation in nozzles and diffusers, J. Sound Vibr. 41(2)207-232(1975)

12. EVERSMAN,W., Acoustic energy in ducts - further observations, J. Sound Vibr. 62(4)517-532(1979)

13. BENJAMIN,T. BROOKE, Effects of a flexible boundary on hydrodynamic stability, J. Fluid Mech. 9(4)513-532(1960)

14. BENJAMIN,T. BROOKE, The threefold classification of unstable disturbances in flexible surfaces bounding inviscid flows, J. Fluid Mech. 16(3)436-450(1963)

15. LANDAHL,M.T., On the stability of a laminar incompressible boundary layer over a flexible surface, J. Fluid Mech. 13(4)609-632(1962)

16. MILES,J.W., On the aerodynamic instability of thin panels. J. Aeronaut. Sci. 23(8)771-780(1956)

17. GUPTA,A.K. et al., Experimental and theoretical investigation of the stability of air flow over a water surface, J. Fluid Mech. 33(4)673-691(1968)

18. MELCHER,J., Continuum electromechanics, MIT Press (1981)

19. BRAZIER-SMITH,P.R. & SCOTT,J.F, The influence of flow on flexural waves. Proc. Inst. of Acoustics Conf. on Advances in Underwater Acoustics, AUWE Portland(1981)

20. LEPPINGTON,F.G. & LEVINE,H., The effect of flow on the piston problem of acoustics, J. Sound Vibr. 62(1)3-17(1979)

21. DOWELL,E.H., Flutter of infinitely long plates and shells. Part I: plates, AIAA J. 4(8)1370-1377(1966)

22. FFOWCS WILLIAMS,J.E. & PURSHOUSE,M., A vortex sheet model of boundary-layer noise, J. Fluid Mech. 113,187-220(1981)

23. HANSEN,R.J. et al., An experimental study of flow-generated waves on a flexible surface, J. Sound Vibr. 68(3)317-334(1980)

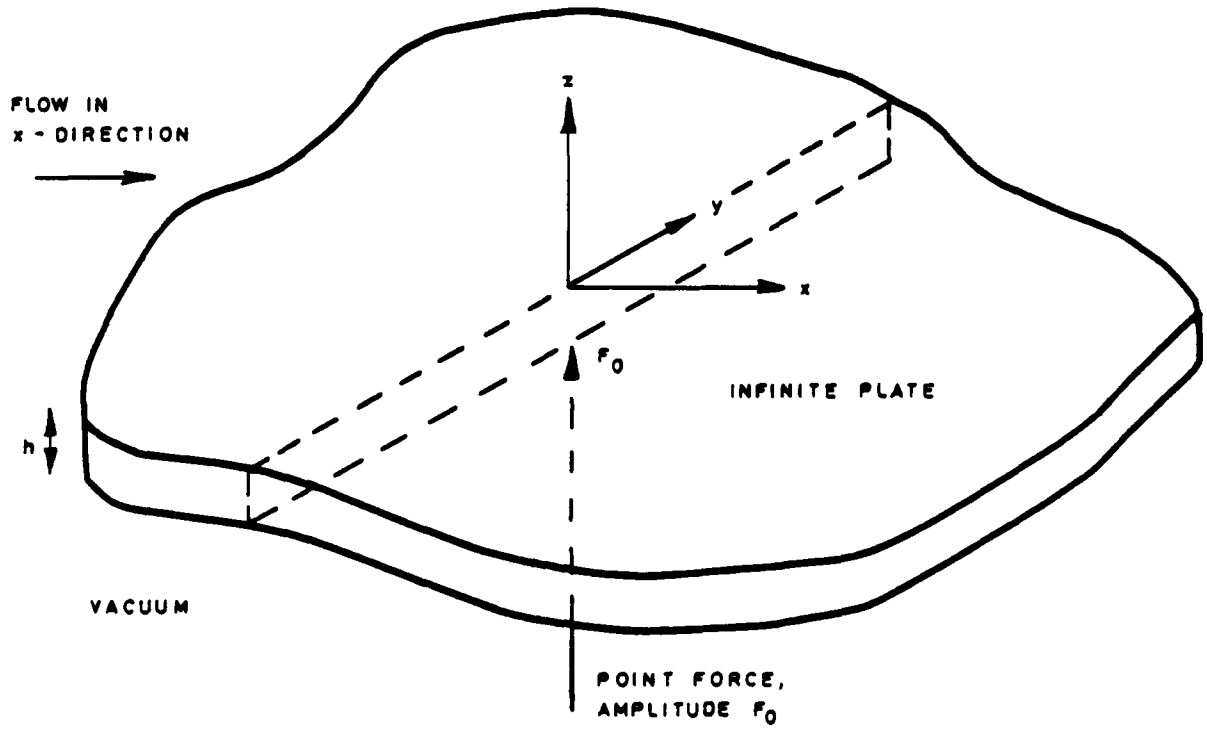

FIG. 1(a) FLOW GEOMETRY, POINT - EXCITED PLATE

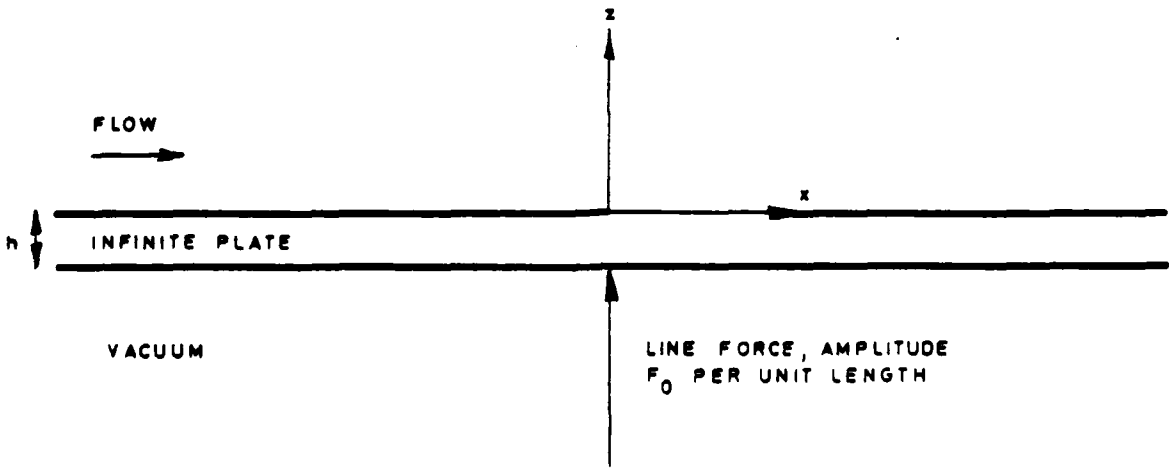

FIG 1(b) FLOW GEOMETRY, LINE - EXCITED PLATE

(a) 'LEPPINGTON AND LEVINE'
CO-ORDINATE SYSTEM
POINT-EXCITED PLATE
FLOW PARALLEL TO x-AXIS
PLATE IN x-y PLANE

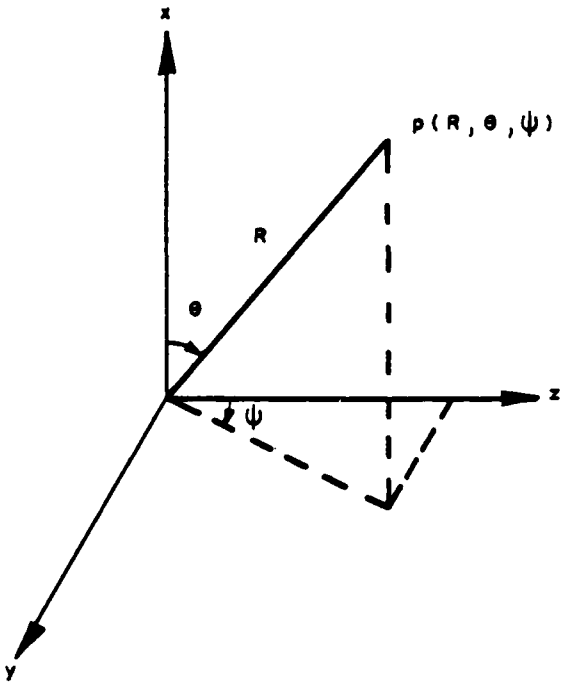

(b) STANDARD CO-ORDINATE
SYSTEM, POINT-EXCITED PLATE
FLOW PARALLEL TO x-AXIS
PLATE IN x-y PLANE

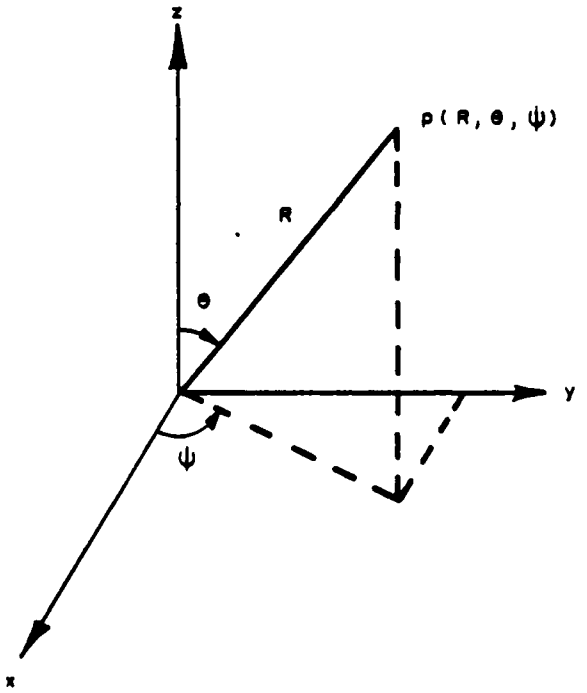

(c) LINE-EXCITED PLATE
FLOW PARALLEL TO x-AXIS
PLATE IN x PLANE

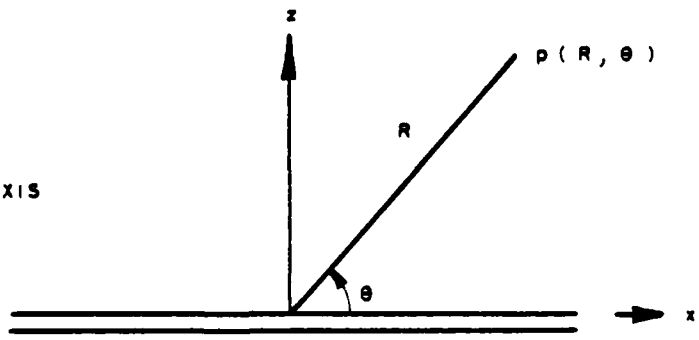

FIG. 2 CO-ORDINATE SYSTEMS FOR FAR-FIELD PRESSURE

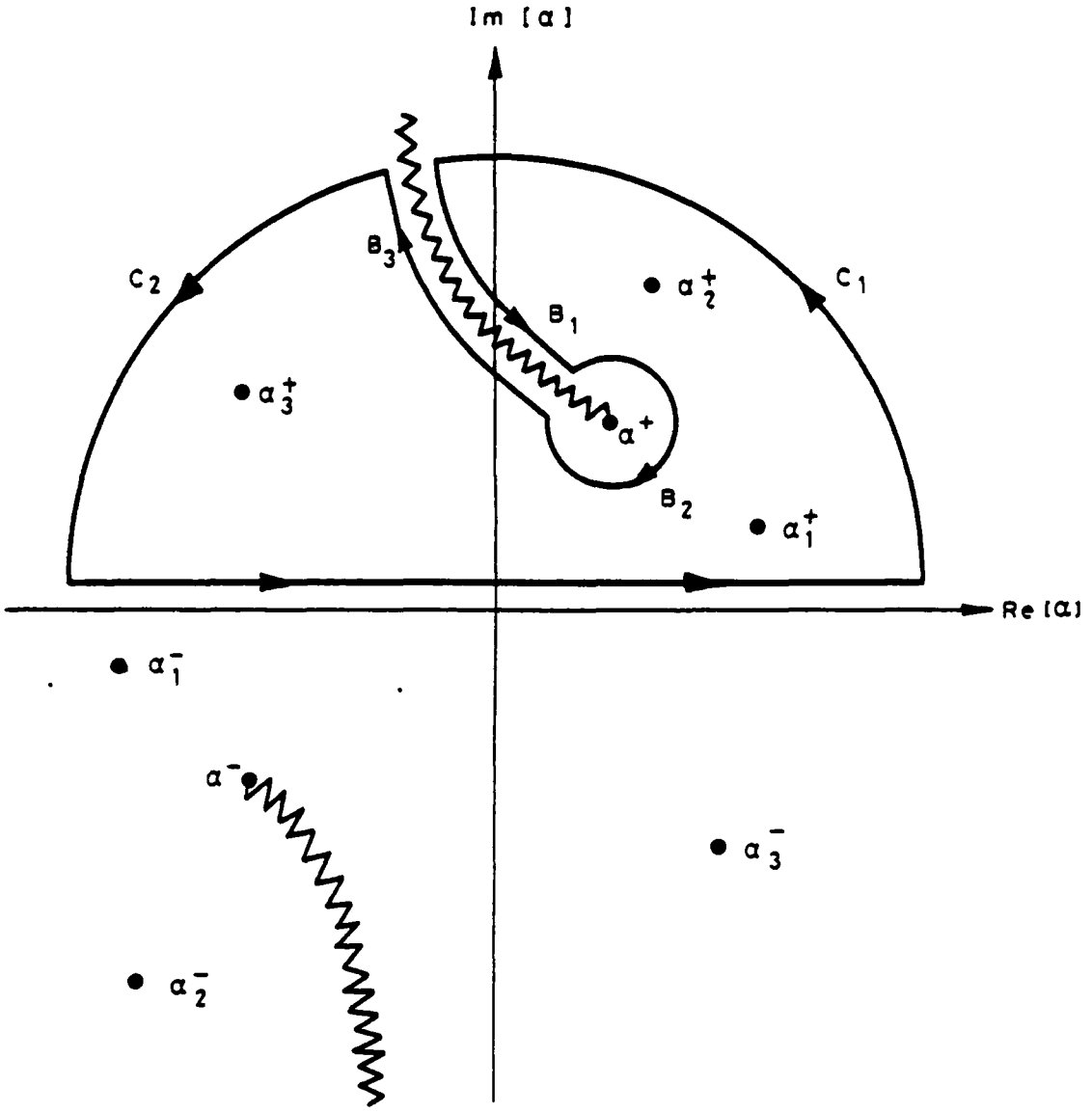

FIG. 3 CLOSURE OF THE FOURIER CONTOUR

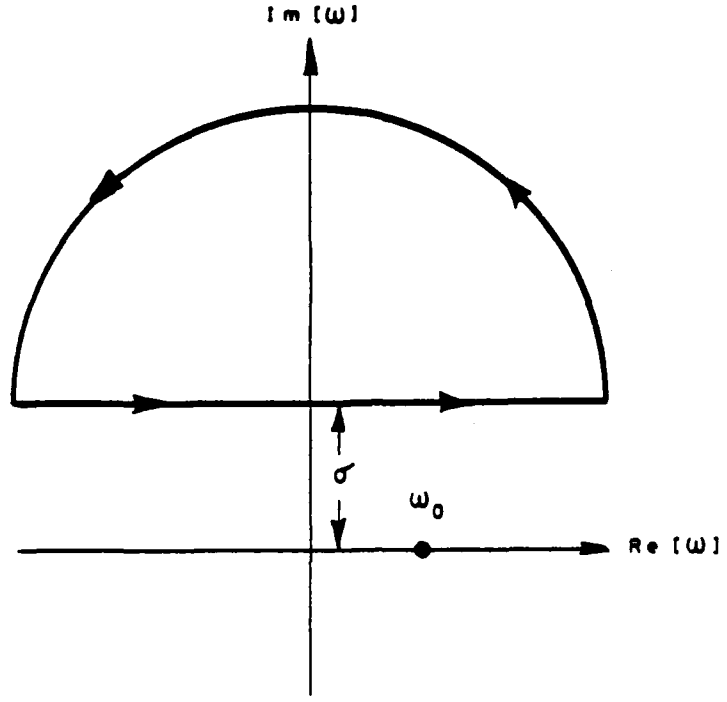

FIG. 4(a) CLOSURE OF THE LAPLACE CONTOUR FOR $t<0$

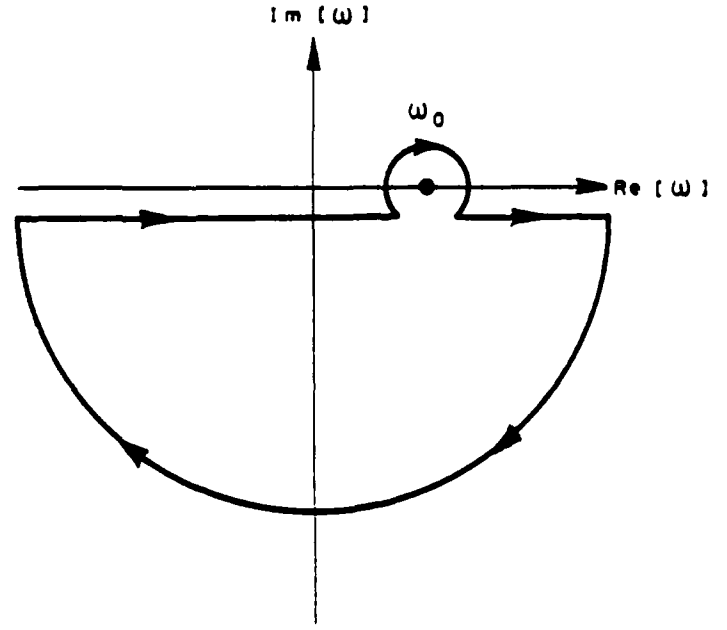

FIG. 4(b) CLOSURE OF THE LAPLACE CONTOUR FOR LARGE $t>0$

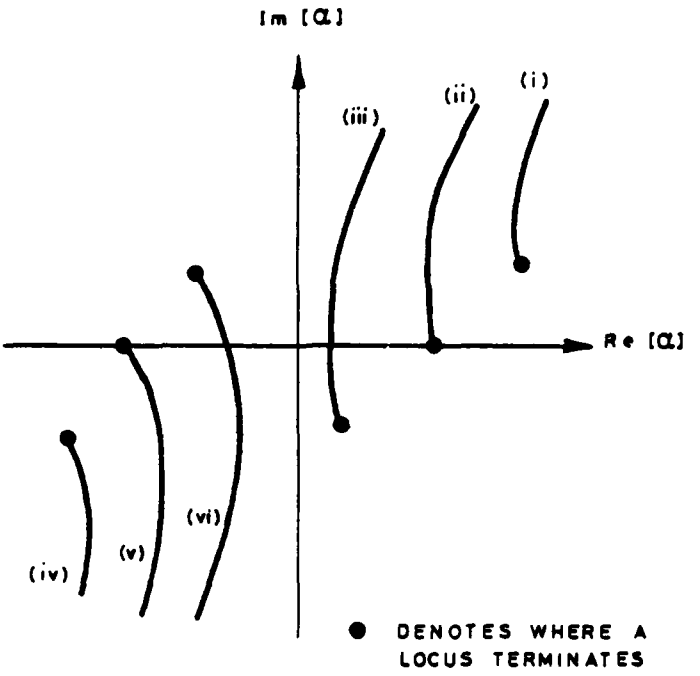

FIG. 5 (a) EXAMPLES OF ROOT LOCI AT A PARTICULAR FREQUENCY ω_0

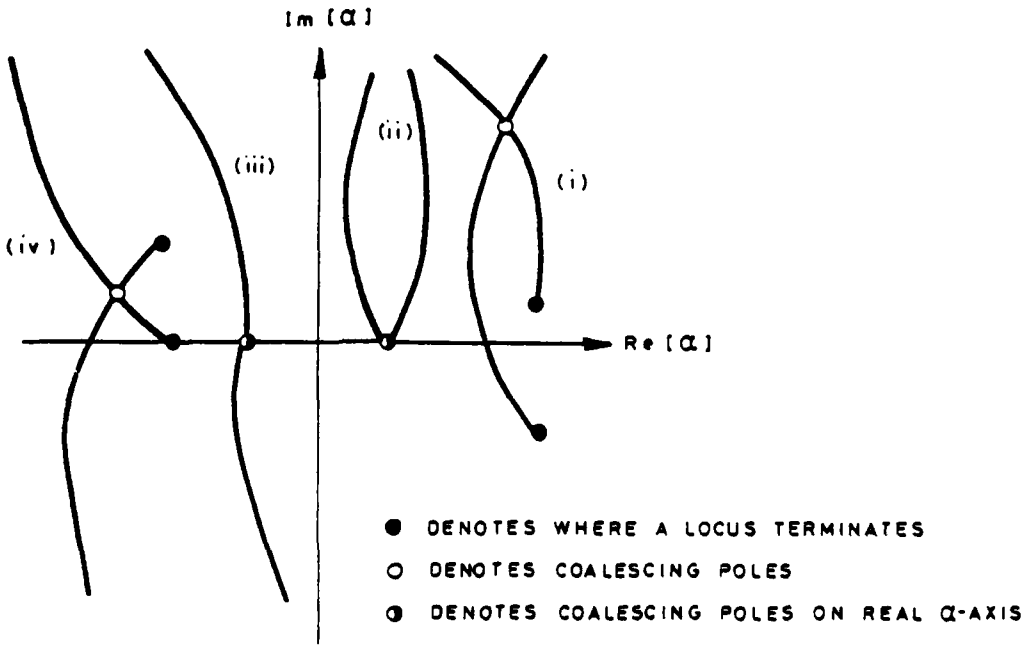

FIG. 5(b) EXAMPLES OF COALESCING POLES

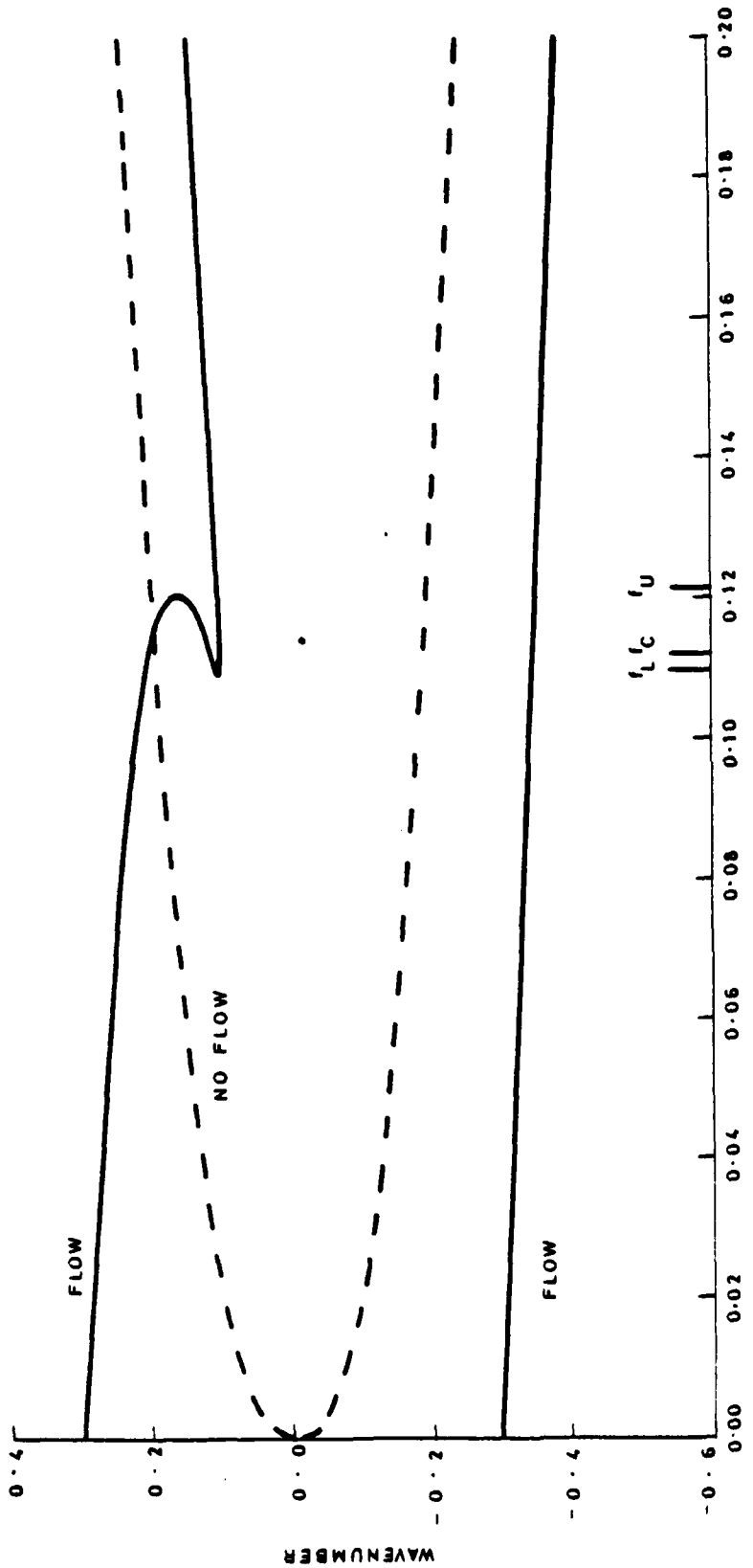

FIG. 6 EFFECT OF 7·5m/s FLOW ON WAVENUMBER-FREQUENCY PLOT

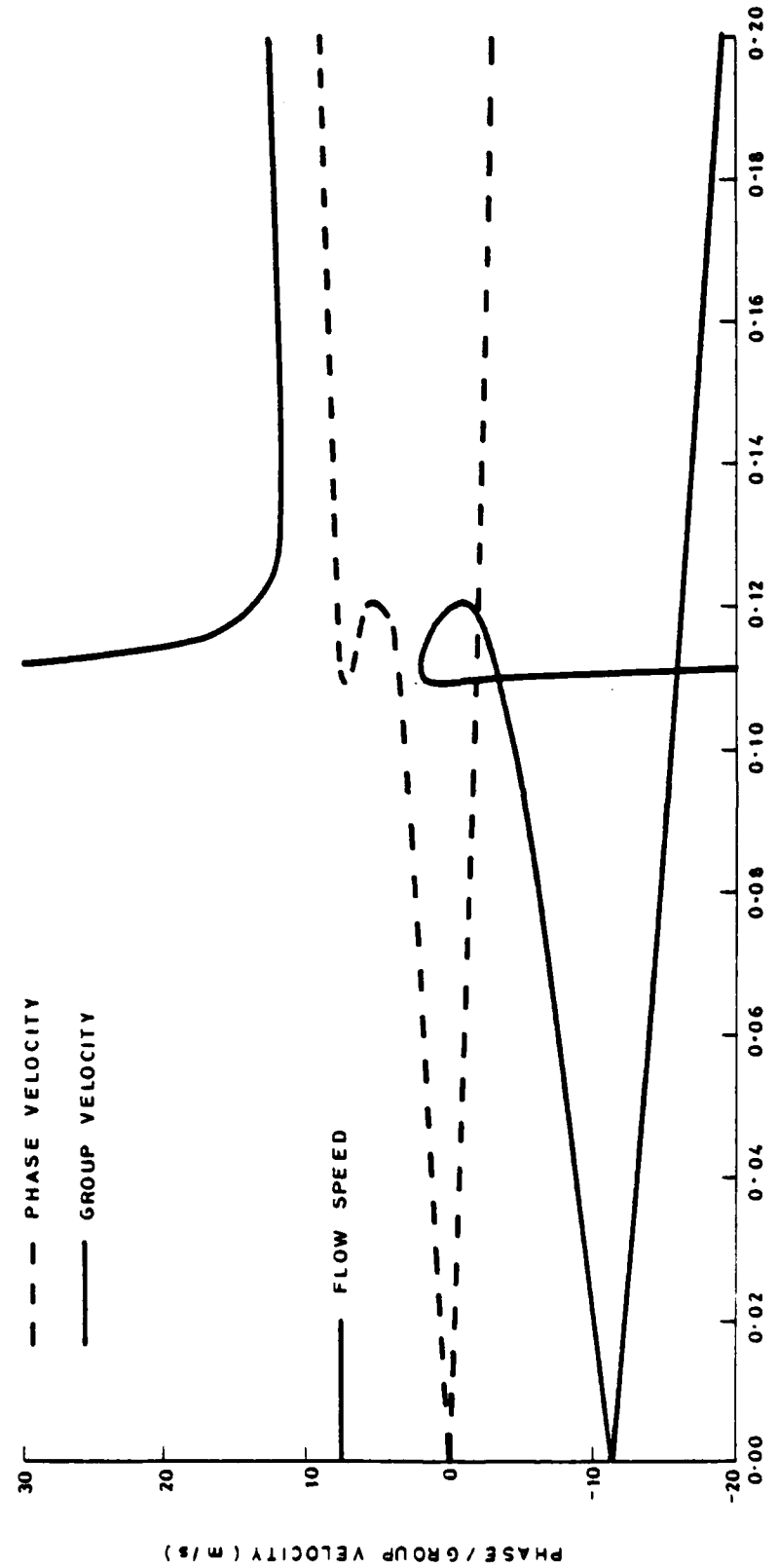

FIG. 7 EFFECT OF 7·5 m/s FLOW ON PHASE AND GROUP VELOCITIES

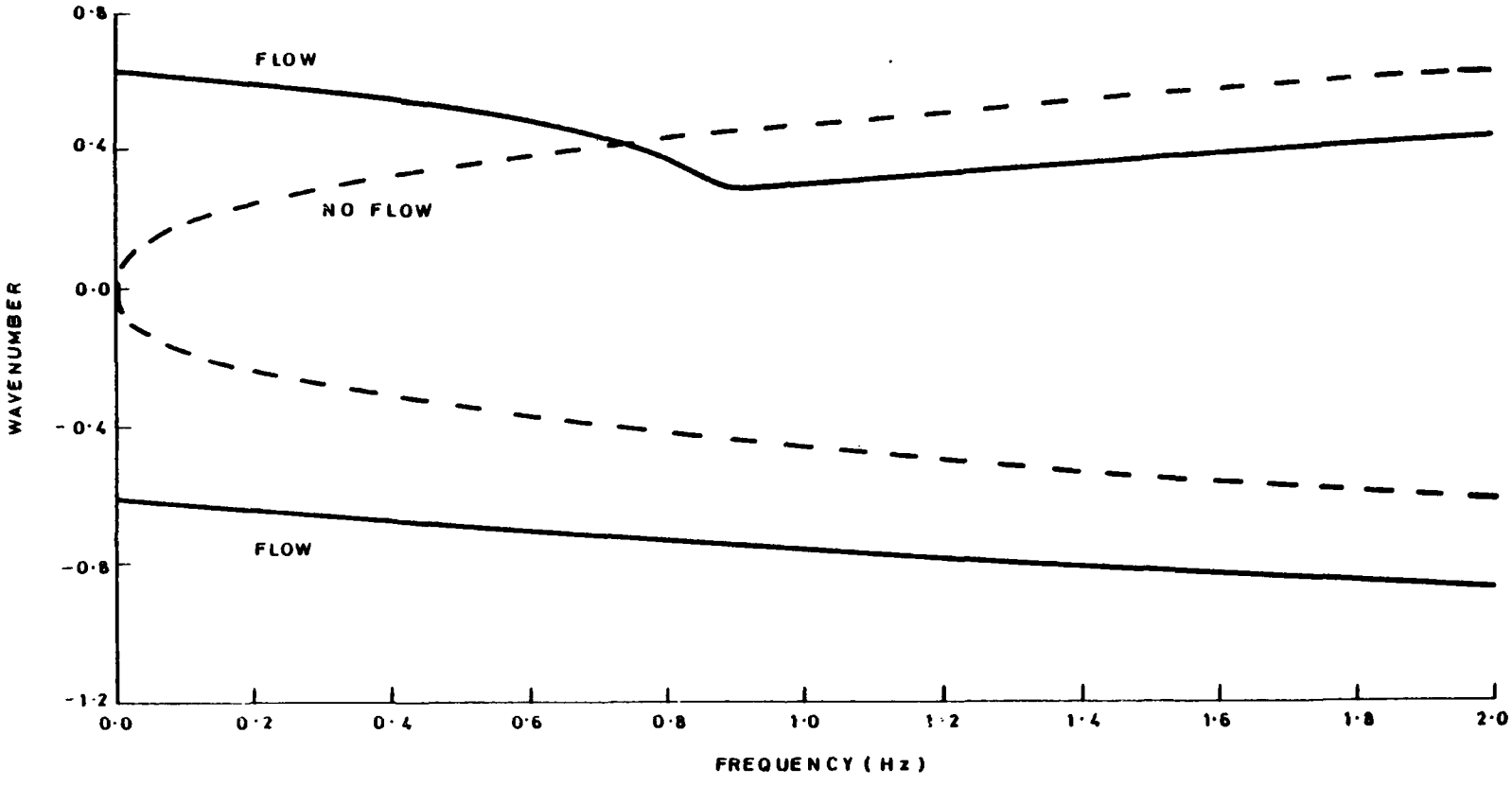

FIG. 8 EFFECT OF 22·5 m/s FLOW ON WAVENUMBER-FREQUENCY PLOT

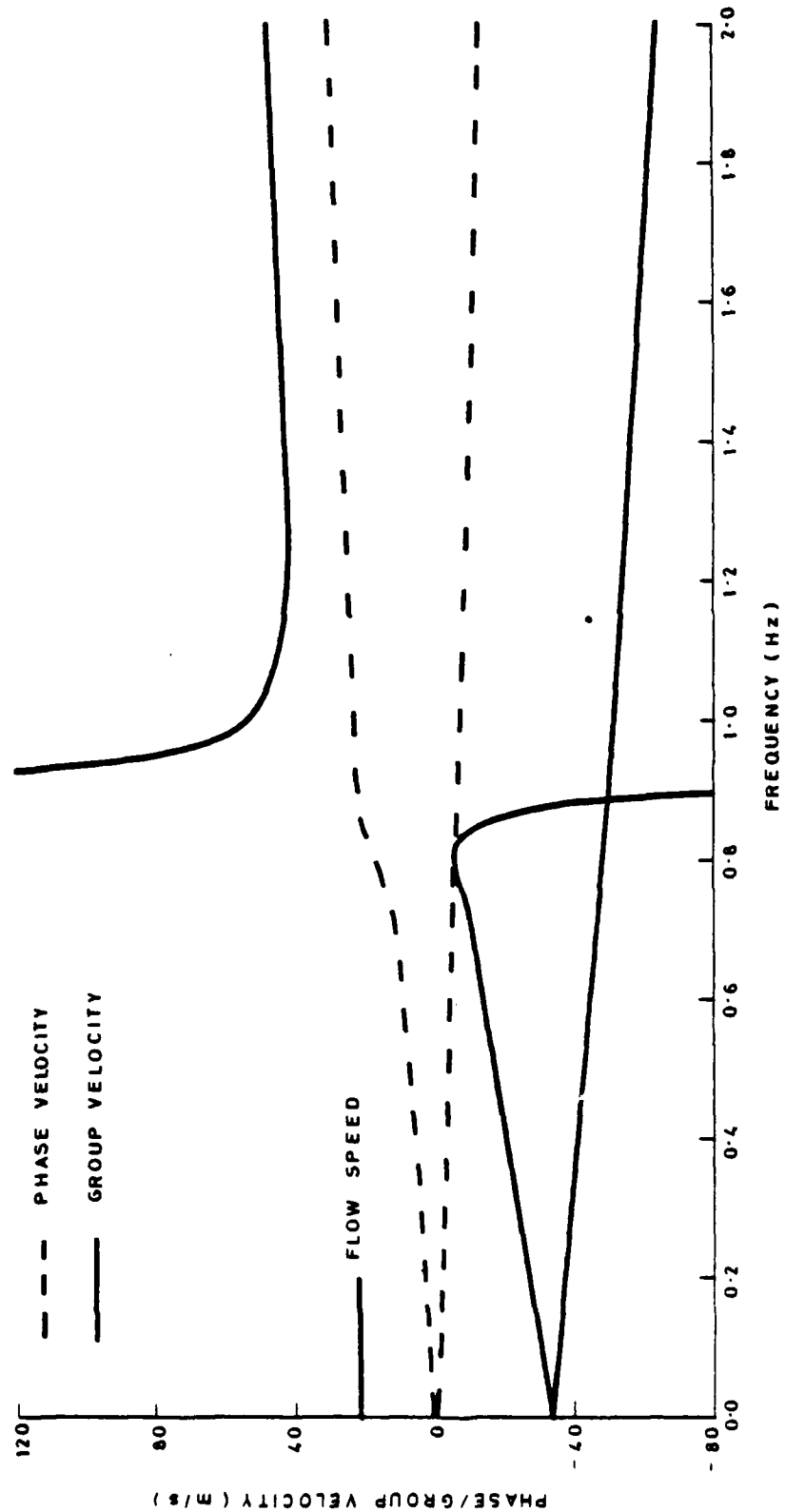

FIG. 9 EFFECT OF 22·5 m/s FLOW ON PHASE AND GROUP VELOCITIES

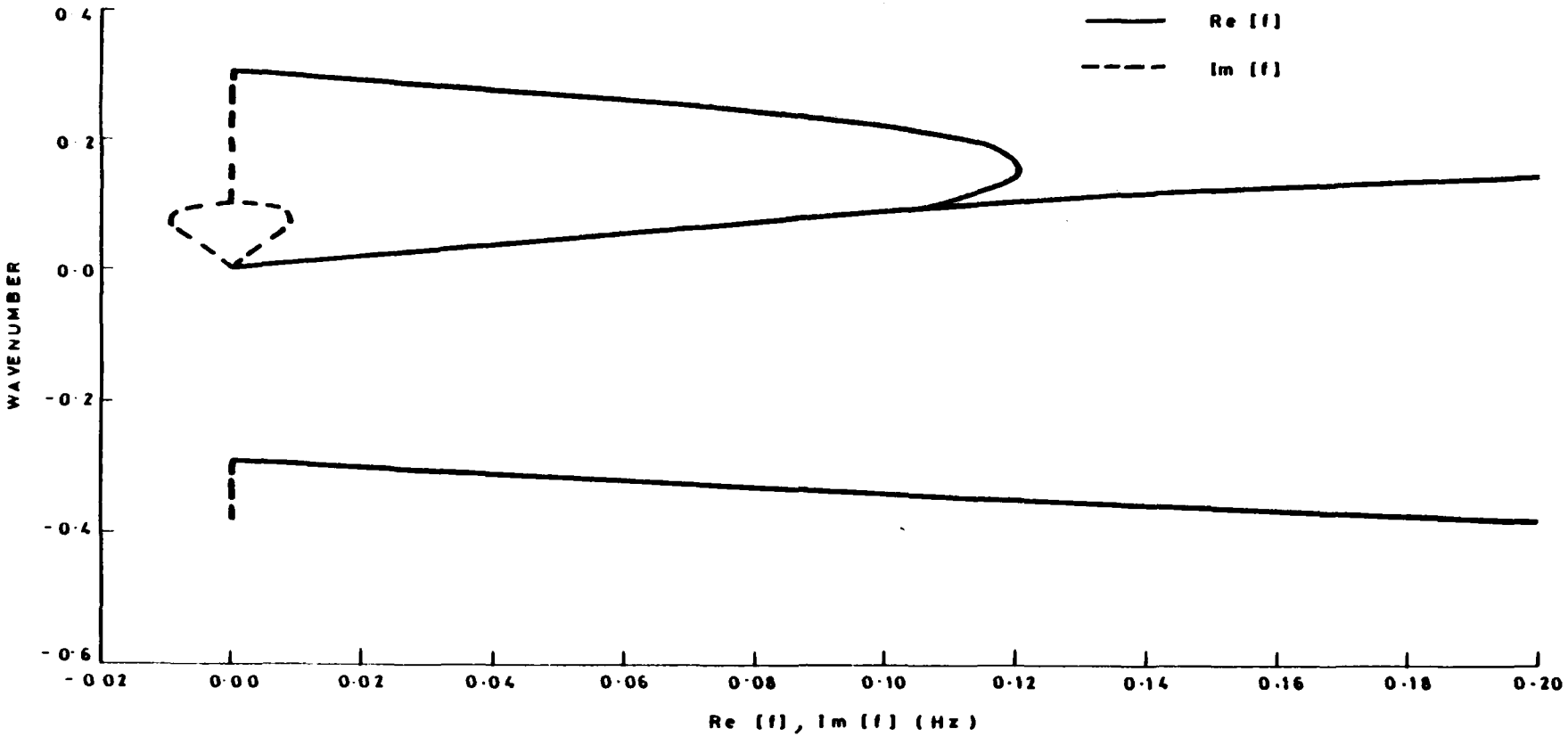

FIG. 10 PLOTS OF WAVENUMBER AGAINST REAL AND IMAGINARY PARTS OF FREQUENCY, U = 7·5 m/s

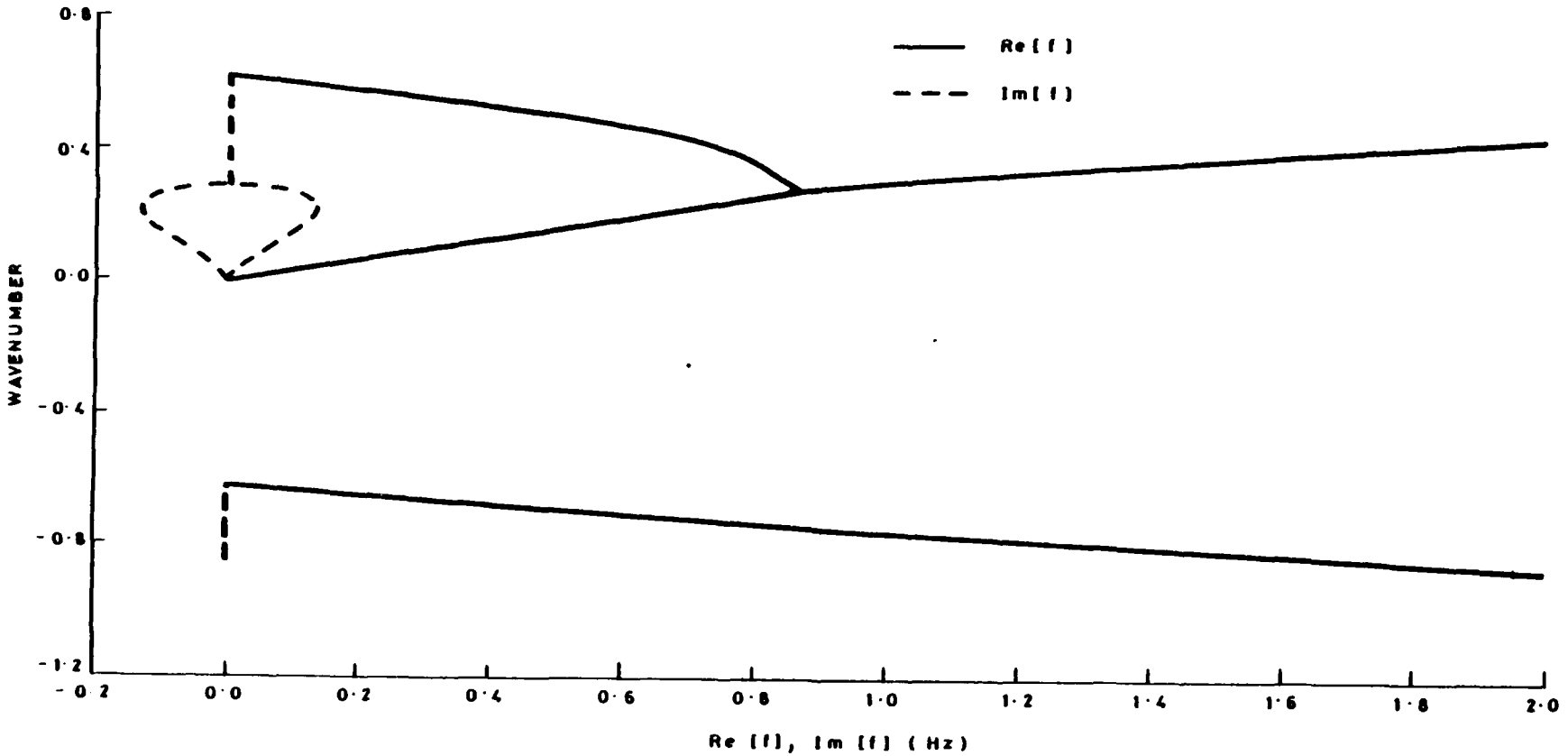

FIG. 11 PLOTS OF WAVENUMBER AGAINST REAL AND IMAGINARY PARTS OF FREQUENCY, U = 22·5 m/s

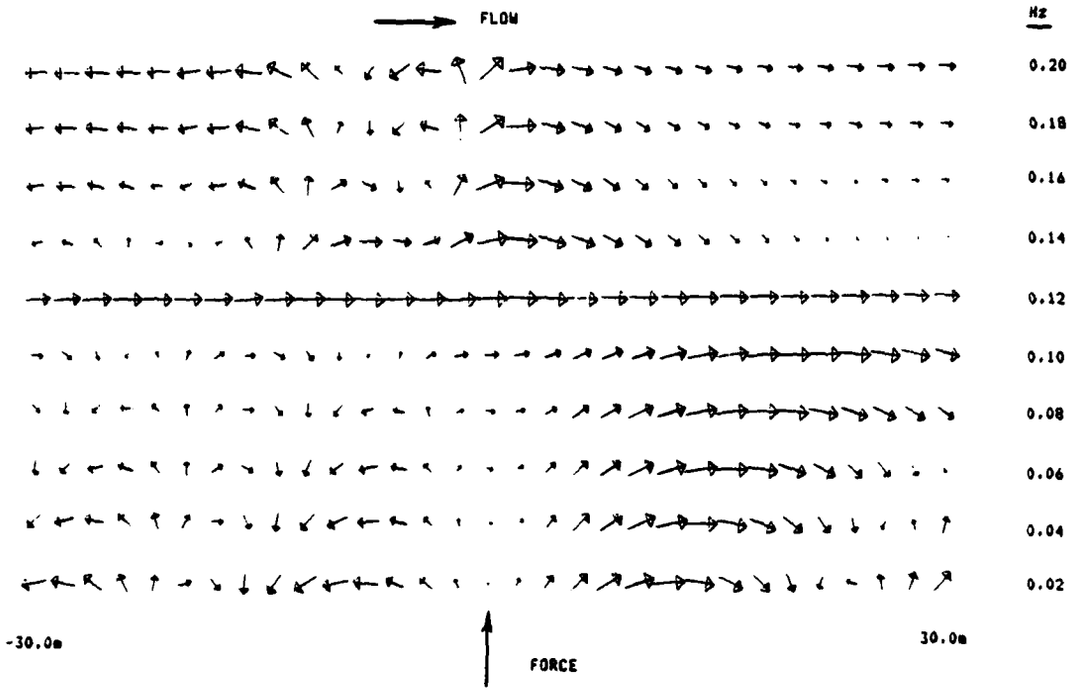

FIG. 12 INTENSITY VECTORS ALONG PLATE SURFACE

U=7.5m/s, FORMULATION 1

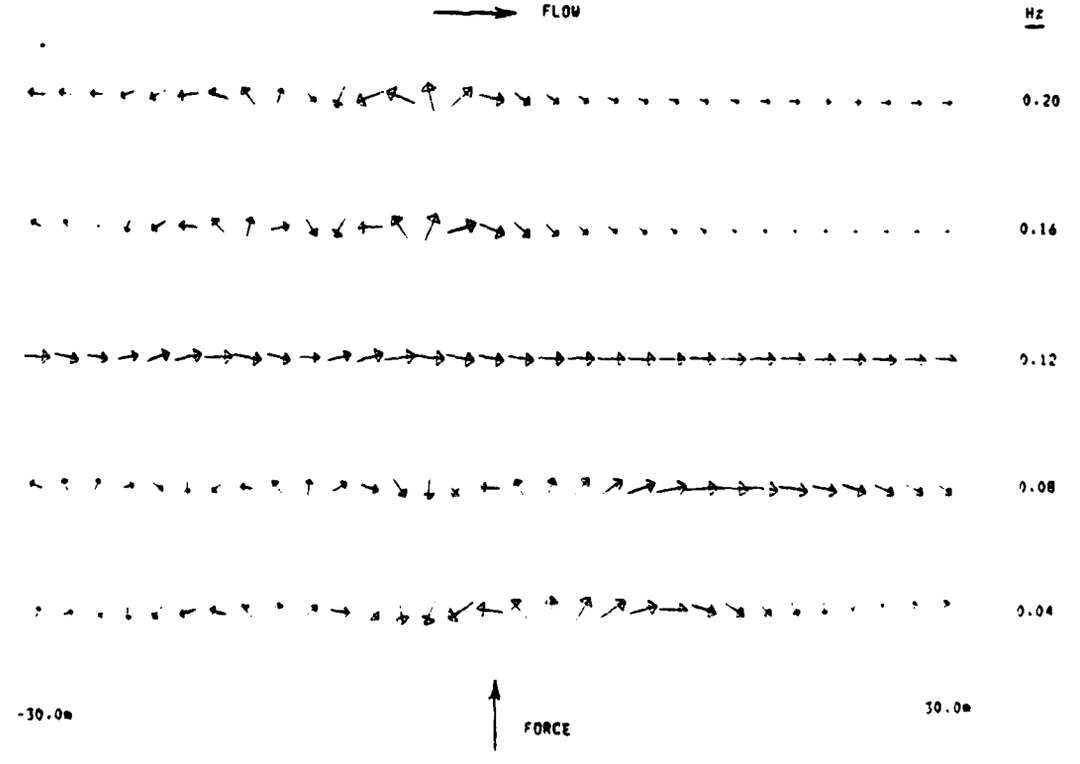

FIG. 13 INTENSITY VECTORS ALONG PLATE SURFACE

U=7.5m/s, FORMULATION 2

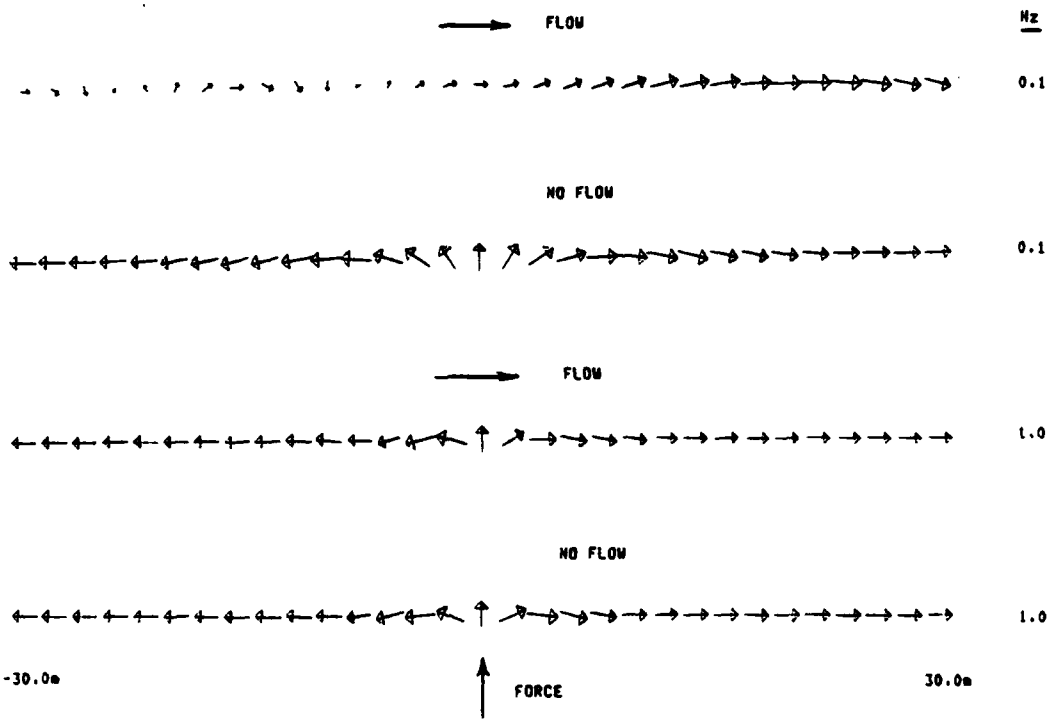

FIG. 14 EFFECT OF 7.5m/s FLOW ON INTENSITY VECTORS ALONG PLATE SURFACE FORMULATION 1

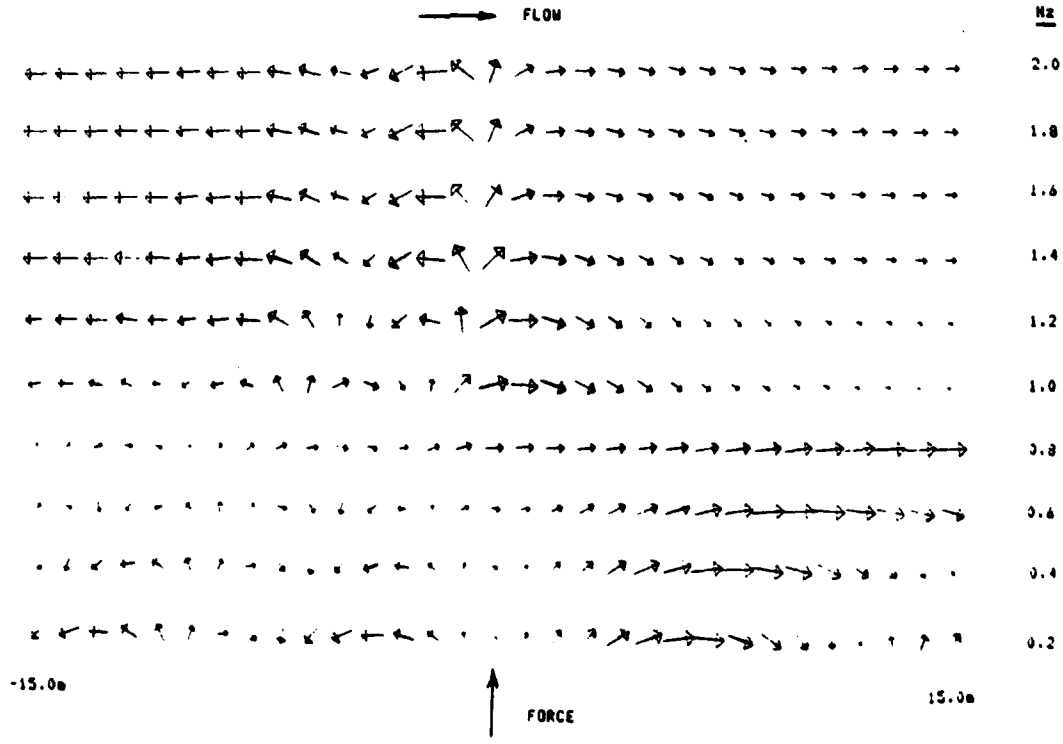

FIG. 15 INTENSITY VECTORS ALONG PLATE SURFACE U=22.5m/s, FORMULATION 1

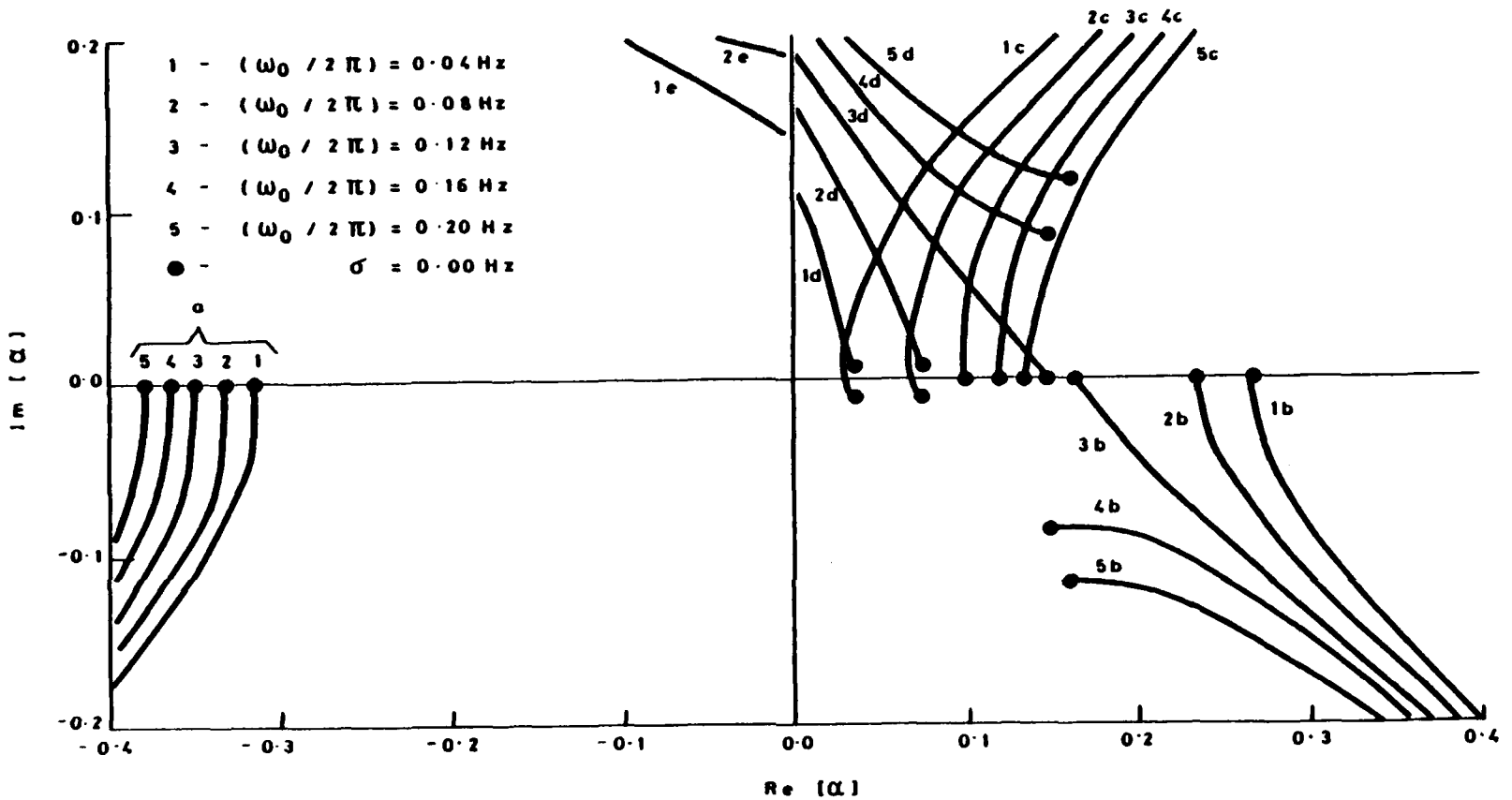

FIG. 16 ROOT LOCI OBTAINED BY VARYING σ FOR VARIOUS VALUES OF ω_0 WITH U = 7·5 m/s, NO DAMPING

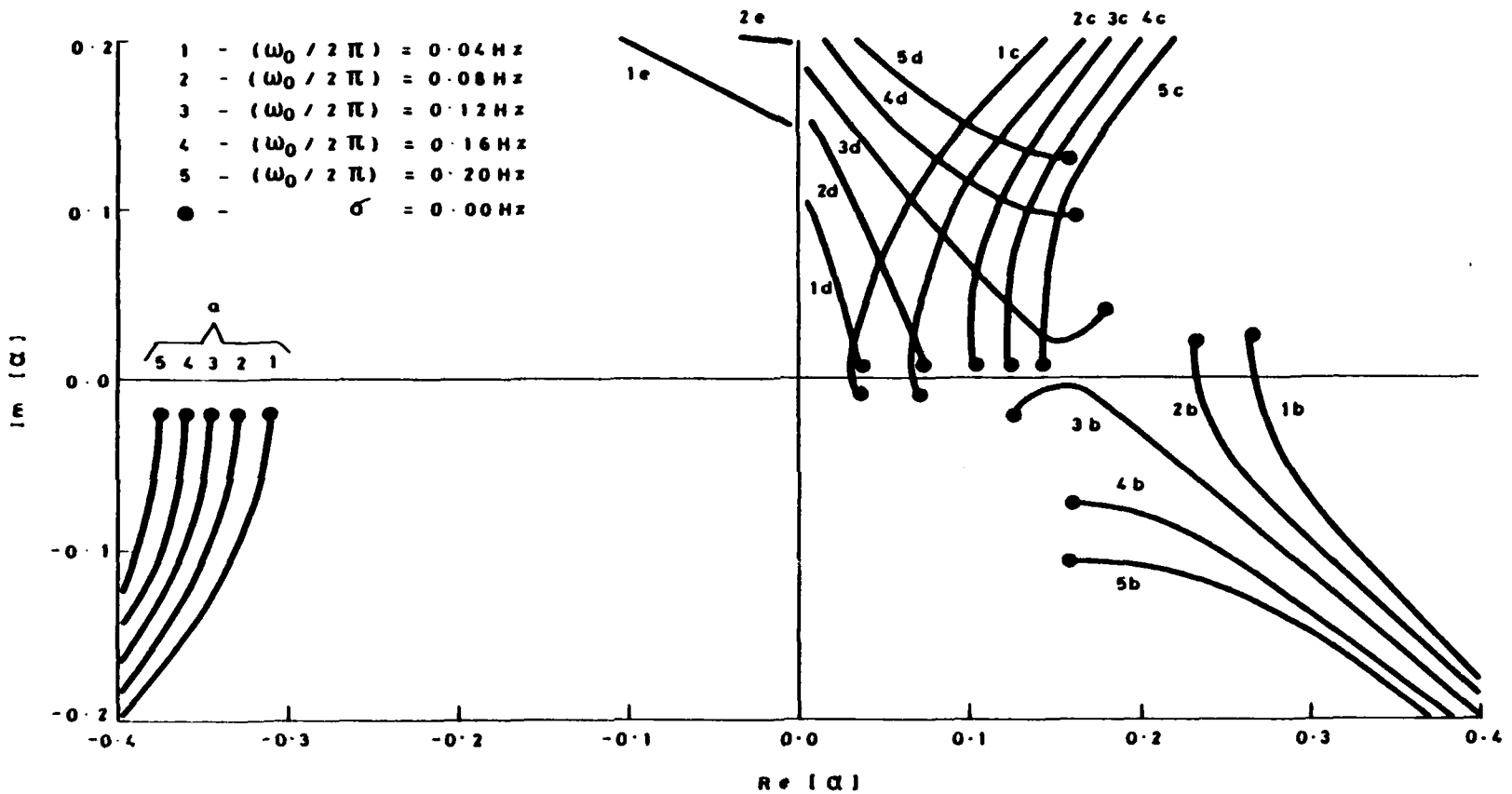

FIG. 17 ROOT LOCI OBTAINED BY VARYING σ FOR VARIOUS VALUES OF ω_0 WITH U = 7·5 m/s AND η = 0·2

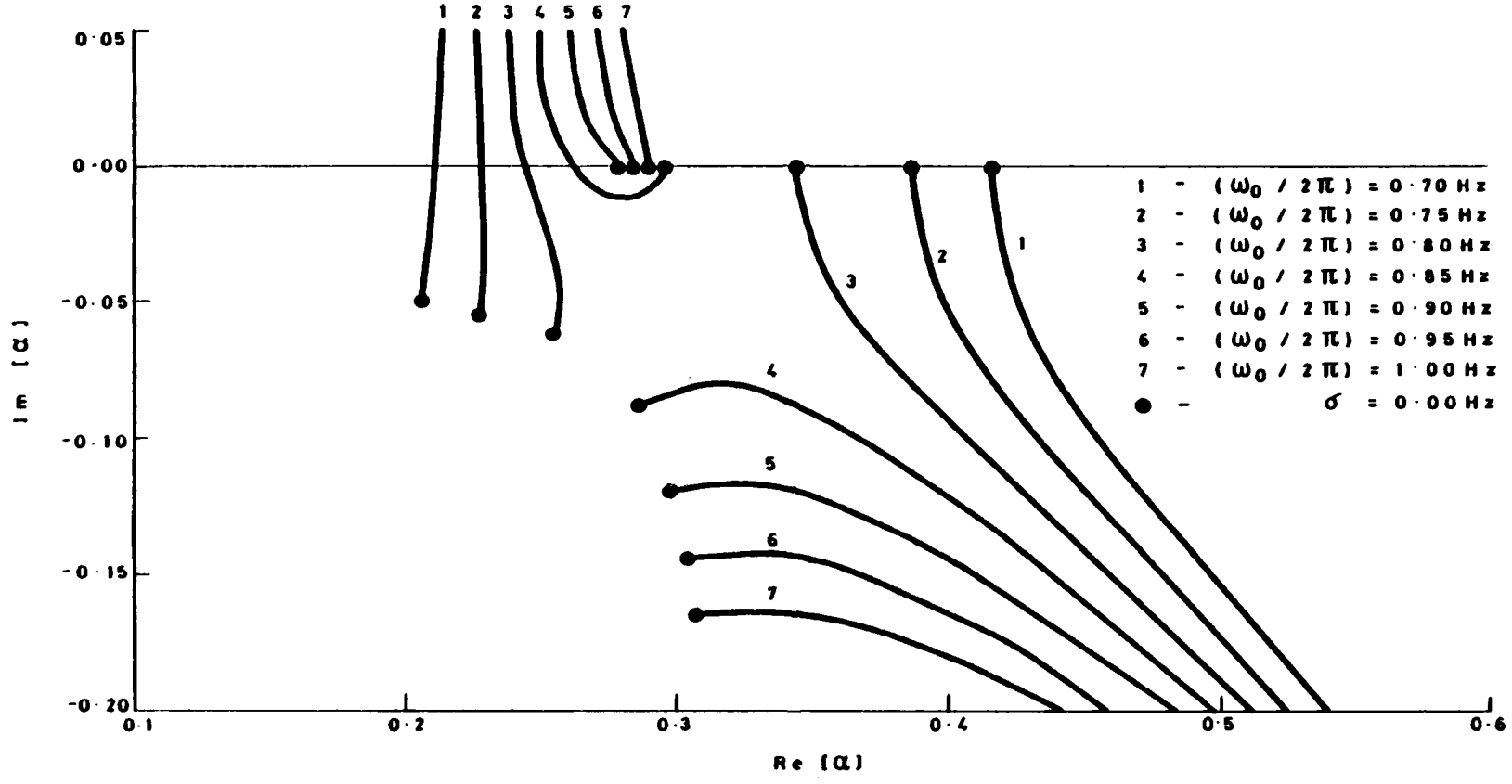

FIG. 18 ROOT LOCI OBTAINED BY VARYING σ FOR VARIOUS VALUES OF ω_0 WITH U = 22·5 m/s, NO DAMPING

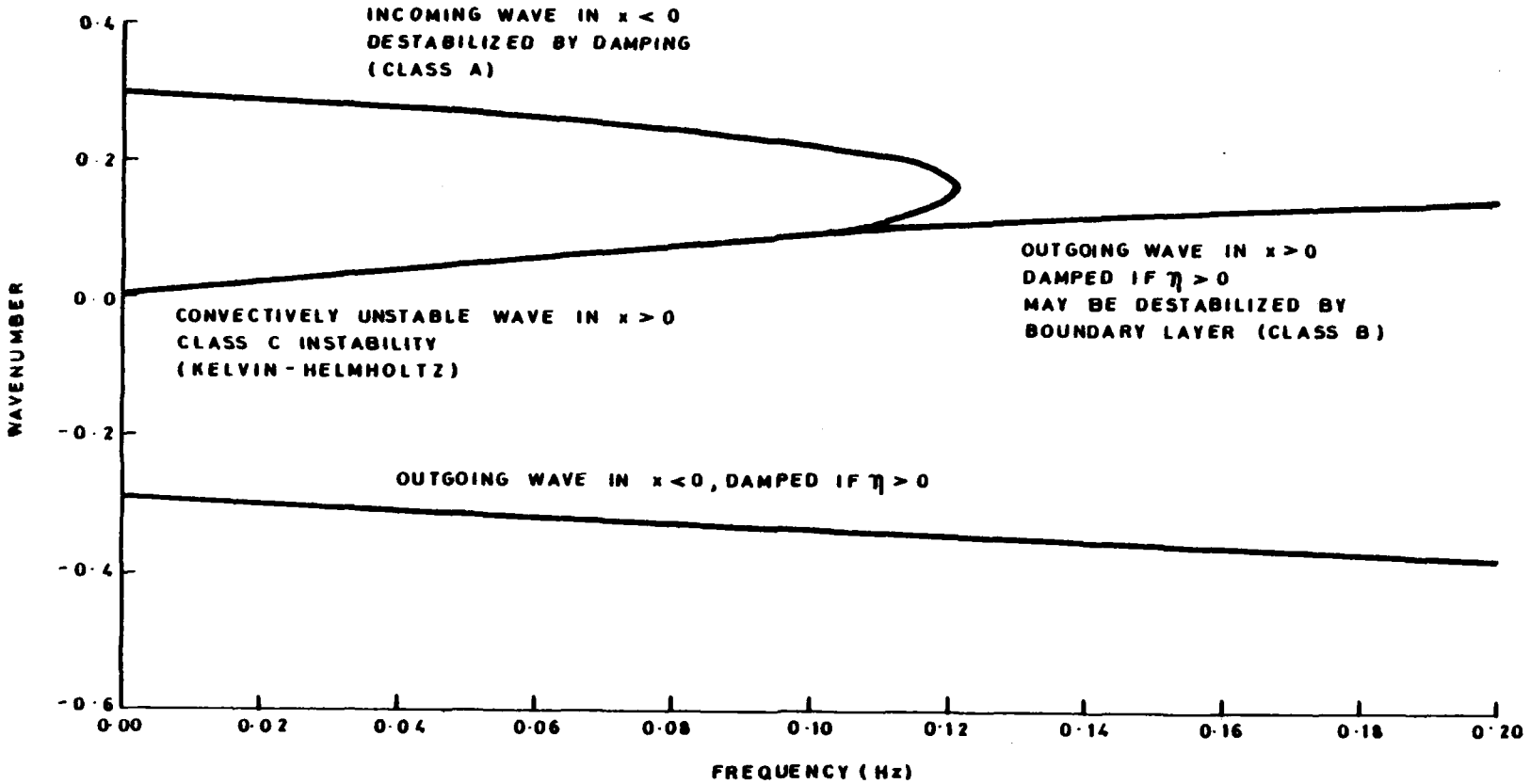

FIG. 19 SUMMARY OF BENJAMIN - LANDAHL [14] AND CAUSAL [19] APPROACHES TO STABILITY, SHOWING INTERPRETATION OF FREE PLATE WAVES

	NO FLOW		U = 7.5 m/s		U = 22.5 m/s	
θ (°)	AMPL. (dB)	PHASE (°)	AMPL. (dB)	PHASE (°)	AMPL. (dB)	PHASE (°)
15.0	103.0	66.2	103.2	54.8	103.5	32.3
30.0	108.6	66.5	108.9	56.4	100.4	36.3
44.0	125.0	89.2	126.1	84.8	128.5	80.2
44.5	126.4	94.5	127.6	91.7	130.0	92.1
45.0	128.0	101.8	129.2	101.5	131.2	108.3
45.5	129.6	112.2	130.7	115.1	131.7	127.7
46.0	131.0	126.8	131.7	132.9	131.2	146.7
46.5	131.8	145.4	131.7	152.8	130.1	162.0
47.0	131.7	165.1	130.9	170.5	128.7	173.3
47.5	130.7	-178.0	129.5	-176.1	127.3	-178.7
48.0	129.3	-165.6	128.1	-166.5	126.0	-172.8
60.0	115.1	-126.1	115.0	-132.0	114.6	-143.4
75.0	112.5	-123.8	112.5	-126.8	112.4	-132.8
90.0	112.3	-123.5	112.3	-123.5	112.3	-123.3
105.0	112.5	-123.8	112.5	-120.7	112.6	-114.2
120.0	115.1	-126.1	115.3	-120.2	115.7	-108.3
131.0	126.5	-150.5	127.6	-147.2	129.9	-145.2
131.5	127.9	-156.8	129.0	-155.3	131.2	-159.1
132.0	129.3	-165.6	130.4	-166.8	132.0	-177.5
132.5	130.7	-178.0	131.6	177.3	131.8	162.6
133.0	131.7	165.1	131.9	157.8	130.6	145.3
133.5	131.8	145.4	131.3	138.6	129.1	132.6
134.0	131.0	126.8	129.9	123.1	127.5	123.7
134.5	129.6	112.2	128.3	112.0	125.9	117.4
135.0	128.0	101.8	126.8	104.2	124.5	113.0
150.0	108.6	66.5	108.3	76.8	107.9	97.7
165.0	103.0	66.2	102.8	77.8	102.5	101.3

TABLE I. FAR-FIELD PRESSURE OF POINT-EXCITED PLATE WITH AND WITHOUT FLOW AT 10 kHz. ψ = 0°.

	NO FLOW		U = 7.5 m/s		U = 22.5 m/s	
θ (°)	AMPL. (dB)	PHASE (°)	AMPL. (dB)	PHASE (°)	AMPL. (dB)	PHASE (°)
15.0	94.8	111.2	94.9	99.8	95.2	77.3
30.0	100.4	111.5	100.6	101.4	101.1	81.3
44.0	116.8	134.2	117.9	129.8	120.2	125.2
44.5	118.2	139.5	119.4	136.7	121.7	137.1
45.0	119.7	146.8	121.0	146.5	123.0	153.3
45.5	121.3	157.2	122.4	160.1	123.5	172.7
46.0	122.8	171.8	123.4	177.9	123.0	-168.3
46.5	123.6	-169.6	123.5	-162.2	121.8	-153.0
47.0	123.4	-149.9	122.6	-144.5	120.4	-141.7
47.5	122.4	-133.0	121.3	-131.1	119.1	-133.7
48.0	121.0	-120.6	119.9	-121.5	117.8	-127.8
60.0	106.9	-81.1	106.7	-87.0	106.4	-98.4
75.0	104.2	-78.8	104.2	-81.8	104.1	-87.8
90.0	104.1	-78.5	104.1	-78.5	104.1	-78.3
105.0	104.2	-78.8	104.3	-75.7	104.4	-69.2
120.0	106.9	-81.1	107.1	-75.2	107.5	-63.3
131.0	118.3	-105.5	119.4	-102.2	121.7	-100.2
131.5	119.6	-111.8	120.8	-110.3	123.0	-114.1
132.0	121.0	-120.6	122.2	-121.8	123.8	-132.5
132.5	122.4	-133.0	123.3	-137.7	123.5	-152.4
133.0	123.4	-149.9	123.7	-157.2	122.4	-169.7
133.5	123.6	-169.6	123.0	-176.4	120.8	177.6
134.0	122.8	171.8	121.7	168.1	119.2	168.7
134.5	121.3	157.2	120.1	157.0	117.7	162.4
135.0	119.7	146.8	118.5	149.2	116.3	158.0
150.0	100.0	111.5	100.1	121.8	99.6	142.7
165.0	94.8	111.2	94.6	122.8	94.3	146.3

TABLE II. FAR-FIELD PRESSURE OF LINE-EXCITED PLATE WITH AND WITHOUT FLOW AT 10 kHz.

A P P E N D I X A

Derivation of the Far-field Sound Pressure of a Point-excited Plate

The general expression for the acoustic pressure amplitude $P(x,y,z)$ of a point-excited plate is given as equation (8)

$$P(x,y,z) = (-i\rho\omega_0^2 F_0/4\pi^2) \iint_{-\infty}^{\infty} \frac{(1-\alpha M/k)^2}{\gamma} \frac{\exp(i\alpha x+i\beta y+i\gamma z)}{Z(\omega_0,\alpha,\beta)}\, d\alpha d\beta \quad (A1)$$

where Z is defined by equation (10), as

$$Z(\omega_0,\alpha,\beta) = D(\alpha^2+\beta^2)^2 - \rho_S h\omega_0^2 - i\rho\omega_0^2(1-\alpha M/k)^2/\gamma \quad (A2)$$

with

$$\gamma = \sqrt{\{(k-\alpha M)^2-\alpha^2-\beta^2\}} \quad (A3)$$

In this Appendix, a non-standard spherical co-ordinate system defined by equation (32) and illustrated as Figure 2(a) is used, viz:

$$x = R\cdot\cos\theta, \quad y = R\cdot\sin\theta\cdot\sin\psi, \quad z = R\cdot\sin\theta\cdot\cos\psi \quad (A4)$$

The double integral given by equation (A1) can be reduced to the form

$$P = \iint_{-\infty}^{\infty} f(\alpha,\beta)\, \exp[iR\cdot g(\alpha,\beta)]\, d\alpha d\beta \quad (A5)$$

According to the method of stationary phase, as $R\to\infty$, then

$$P \simeq 2\pi i s\cdot f(\alpha_0,\beta_0)\cdot\exp[iR\cdot g(\alpha_0,\beta_0)]/[R\sqrt{|ab-d^2|}] \quad (A6)$$

where the stationary phase point (α_0,β_0) is given by the simultaneous solution of

$$\partial g/\partial\alpha = \partial g/\partial\beta = 0 \quad (A7)$$

In addition, let

$$a = \partial^2 g/\partial\alpha^2, \quad b = \partial^2 g/\partial\beta^2, \quad d = \partial^2 g/\partial\alpha\partial\beta \tag{A8}$$

where the derivatives are evaluated at (α_0,β_0). Then

$$s = +1, \quad ab>d^2, \quad a>0 \tag{A9-1}$$

$$s = -1, \quad ab>d^2, \quad a<0 \tag{A9-2}$$

$$s = -i, \quad ab<d^2 \tag{A9-3}$$

In terms of the spherical co-ordinate system given by equation (A4), the exponent g is given by

$$g(\alpha,\beta) = \alpha\cdot\cos\theta + \beta\cdot\sin\theta\cdot\sin\psi + \sqrt{(k'^2-\beta^2)}\cdot\sin\theta\cdot\cos\psi \tag{A10}$$

where

$$k' = k'(\alpha) = \sqrt{[(k-\alpha M)^2-\alpha^2]} \tag{A11}$$

and the first derivatives of g are given by

$$\partial g/\partial\alpha = \cos\theta - [\{\alpha+(k-\alpha M)M\}/\sqrt{(k'^2-\beta^2)}]\cdot\sin\theta\cdot\cos\psi \tag{A12}$$

$$\partial g/\partial\beta = [-\beta/\sqrt{(k'^2-\beta^2)}]\cdot\sin\theta\cdot\cos\psi + \sin\theta\cdot\sin\psi \tag{A13}$$

Setting $(\partial g/\partial\beta)=0$ gives

$$\tan\psi = \beta_0/\sqrt{(k'^2-\beta_0^2)} \tag{A14}$$

which in turn gives the result

$$\beta_0 = k'(\alpha_0)\cdot\sin\psi \tag{A15}$$

Substituting equation (A15) into equation (A12) gives

$$\partial g/\partial \alpha = \cos\theta - [\{\alpha+(k-\alpha M)M\}/k']\cdot\sin\theta \qquad (A16)$$

which results in

$$\tan\theta = \sqrt{[(k-\alpha_0 M)^2-\alpha_0^2]}/[\alpha_0+(k-\alpha_0 M)M] \qquad (A17)$$

This equation has a closed-form solution

$$\alpha_0 = [k/(1-M^2)][-M + \cos\theta \,/\, \sqrt{(1-M^2\sin^2\theta)}] \qquad (A18)$$

Substituting equation (A18) into equations (A11) and (A15) gives

$$\beta_0 = k\cdot\sin\theta\cdot\sin\psi \,/\, \sqrt{(1-M^2\sin^2\theta)} \qquad (A19)$$

In addition,

$$\gamma(\alpha_0,\beta_0) = k\cdot\sin\theta\cdot\cos\psi \,/\, \sqrt{(1-M^2\sin^2\theta)} \qquad (A20)$$

and

$$g(\alpha_0,\beta_0) = [k/(1-M^2)][-M\cdot\cos\theta + \sqrt{(1-M^2\sin^2\theta)}] \qquad (A21)$$

The second derivatives of g are given by

$$\partial^2 g/\partial\alpha^2 = -\sin\theta\cdot\cos\psi\ [k^2-(1-M^2)\beta^2] \,/\, (k'^2-\beta^2)^{3/2} \qquad (A22)$$

$$\partial^2 g/\partial\beta^2 = -\sin\theta\cdot\cos\psi\cdot k'^2/(k'^2-\beta^2)^{3/2} \qquad (A23)$$

$$\partial^2 g/\partial\alpha\partial\beta = -\sin\theta\cdot\cos\psi\cdot\beta[\alpha+(k-\alpha M)M] \,/\, (k'^2-\beta^2)^{3/2} \qquad (A24)$$

By evaluating the expressions (A22) to (A24) at (α_0,β_0), it can be shown that

$$ab-d^2 = (1-M^2\sin^2\theta) \,/\, (k^2\sin^2\theta\cdot\cos^2\psi) \qquad (A25)$$

and

$$b = -\sqrt{(1-M^2\sin^2\theta)} \,/\, (k\cdot\cos^2\psi) \qquad (A26)$$

From equations (A26) and (A27), it is evident that $ab-d^2>0$ and $b<0$. Hence $a<0$ and $s=-1$, from which equation (A6) becomes

$$P \approx (-2\pi ik)\cdot\sin\theta\cdot\cos\psi\cdot\exp[iR\cdot g(k,M,\theta)]\cdot f(\alpha_0,\beta_0)/(1-M^2\sin^2\theta) \qquad (A27)$$

By expressing $f(\alpha_0,\beta_0)$ and $g(\alpha_0,\beta_0)$ in terms of k, M, θ and ψ, some algebraic manipulation gives the result (equation (36)) for the far-field pressure.

APPENDIX B

Far-field Sound Pressure of a Point-excited Plate Expressed in Traditional Spherical Co-ordinates

The co-ordinate system is defined by

$$x = R\cdot\sin\theta\cdot\cos\psi, \quad y = R\cdot\sin\theta\cdot\sin\psi, \quad z = R\cdot\cos\theta \tag{B1}$$

The stationary phase point (α_0,β_0) is given by

$$\alpha_0 = [k/(1-M^2)][-M + \sin\theta\cdot\cos\psi \;/\; \sqrt{\{h(M,\theta,\psi)\}}] \tag{B2}$$

$$\beta_0 = k\cdot\sin\theta\cdot\sin\psi \;/\; \sqrt{\{h(M,\theta,\psi)\}} \tag{B3}$$

where

$$h(M,\theta,\psi) = 1 - M^2(1 - \sin^2\theta\cdot\cos^2\psi) \tag{B4}$$

The far-field pressure is given by

$$P(R,\theta,\psi) = \frac{F_0\left[\frac{-ik}{2\pi R}\right](1-\alpha_0 M/k)^2\left[\frac{\cos\theta}{h(M,\theta,\psi)}\right]\exp\{iR\cdot g(k,M,\theta,\psi)\}}{(1-\alpha_0 M/k)^2 - \left[\frac{ik\cdot\cos\theta}{\mu\cdot\sqrt{\{h(M,\theta,\psi)\}}}\right]\{1-(\alpha_0^2+\beta_0^2)^2/k_p^4\}} \tag{B5}$$

where

$$g(k,M,\theta,\psi) = [k/(1-M^2)][-M\cdot\sin\theta\cdot\cos\psi + \sqrt{\{h(M,\theta,\psi)\}}] \tag{B6}$$

END

FILMED

3-83

DTIC